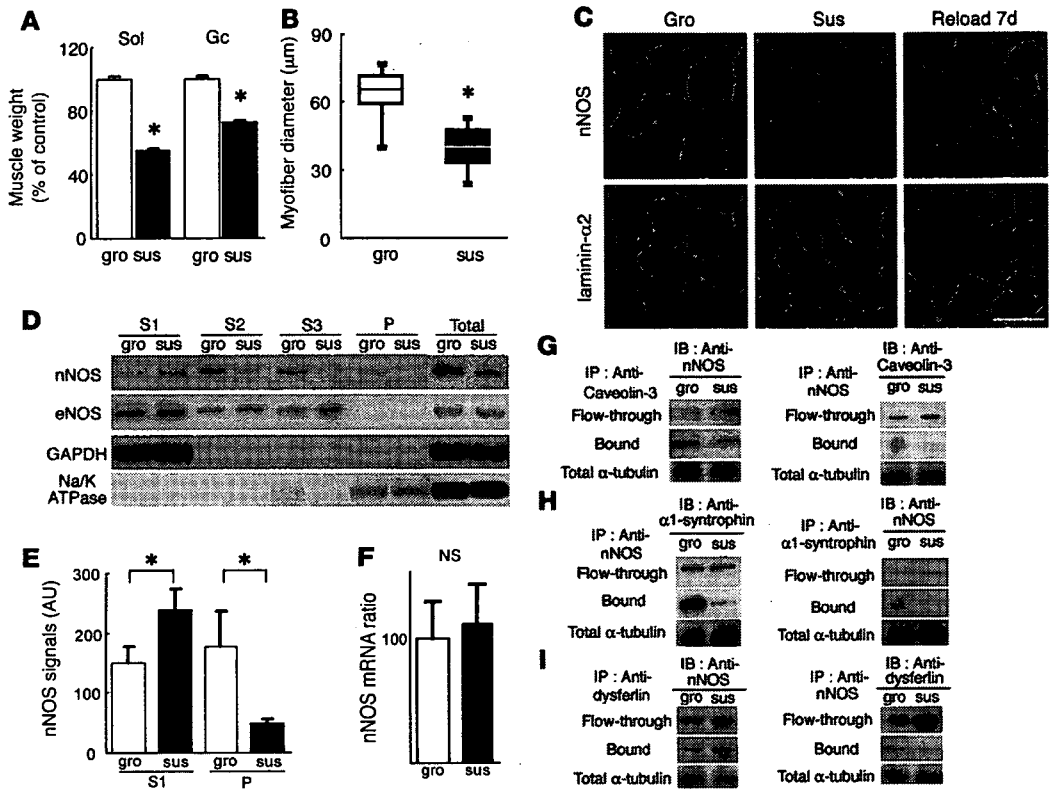

Figure 1

nNOS disappears from the sarcolemma during tail suspension. (**A**) Weights of soleus (Sol) and gastrocnemius (Gc) muscles from tail-suspended (sus) wild-type mice are normalized to body weight and are expressed as percentage of ground control (gro) (n = 15/group). *P < 0.05, Student's t test. (**B**) Box and whiskers plot of myofiber diameter size of soleus. Boxes represent the middle 50% of the data, lines represent the median, and whiskers represent the range. More than 200 fibers were measured on laminin-α2 chain–stained cross sections. (**C**) Immunofluorescent staining for nNOS and laminin-α2 chain. Transverse muscle sections from ground control mice, tail-suspended mice, and mice after reloading for 7 days (reload 7d) were stained with anti-nNOS (green) and anti–laminin-α2 chain antibodies (red). Scale bar: 50 μm. (**D**) Western blot using anti-nNOS antibody on subcellular fractions of muscle extracts. P indicates insoluble pellet after sequential extraction of skeletal muscle homogenates with 100 mM NaCl (S1), 500 mM NaCl (S2), and 0.5% Triton X-100 (S3). GAPDH signals in S1 and Na/K-ATPase signals in P confirmed that our fractionation was correctly done. Fractionation and western blotting were repeated 5 times, and representative data are presented. Note the slight increase of nNOS levels in S1 fraction and loss of nNOS signal in insoluble P fraction during tail suspension. (**E**) Quantification of nNOS signals in S1 and P fractions of muscle extracts shown in D (n = 5 /group). The signals in S1 and P fractions were normalized to GAPDH or Na/K-ATPase, respectively. Mann-Whitney, *P < 0.05. (**F**) Levels of nNOS mRNA in muscles from ground control mice and tail-suspended mice for 2 weeks were evaluated by real-time PCR (n = 5/group). No significant difference was found by Mann-Whitney test. (**G**) Immunoprecipitation with caveolin-3 antibody and immunoblot with nNOS antibody, and vice versa, for ground control and tail suspension groups. (**H**) Immunoprecipitation with α1-syntrophin Ab and immunoblot with nNOS antibody, and vice versa. (**I**) Immunoprecipitation of dysferlin antibody and immunoblot with nNOS Ab, and vice versa. In **G–I**, flow-through fraction was also examined by western blotting with anti–α-tubulin antibody.

inhibitor, 7-nitroindazole (7NI), significantly attenuates suspension-induced muscle atrophy. Furthermore, we show the involvement of nNOS in denervation-induced muscle atrophy process. Thus nNOS and NO are to our knowledge new therapeutic targets for disuse-induced muscle atrophy.

Results

nNOS disappears from the sarcolemma during tail suspension. To elucidate molecular mechanisms of unloading-induced muscle atrophy, we performed tail suspension (14 days) and reloading (7 days) experiments using wild-type C57BL/6 mice. The weights of the soleus and gastrocnemius (Figure 1A) muscles were decreased to 50%–70% of those of the control mice after tail suspension. The mice showed weakened grasping power and less endurance in running on the rotarod test after tail suspension (Supplemental Figure 1; supplemental material available online with this article; doi:10.1172/JCI30654DS1). The diameter of myofiber was also drastically decreased (Figure 1B). The expression patterns of the components of DGC, dystrophin, β-dystroglycan, α-sarcoglycan, dystrobrevin, laminin-α2, α1-syntrophin, and caveolin-3 were not changed during tail suspension (data not shown). The serum creatine kinase level was not elevated, and Evans blue dye uptake by myofibers was not evident in atrophied muscles (Supplemental Figure 2), indicating that the sarcolemmal integrity was maintained during tail suspension. nNOS mRNA levels were not significantly reduced (Figure 1F), and total nNOS protein was slightly decreased during tail suspension (Figure 1D). Importantly, immunohistochemistry revealed that nNOS was lost from the sarcolemma during tail suspension (Figure 1C). The sarcolemmal expression was gradually restored during the reloading process

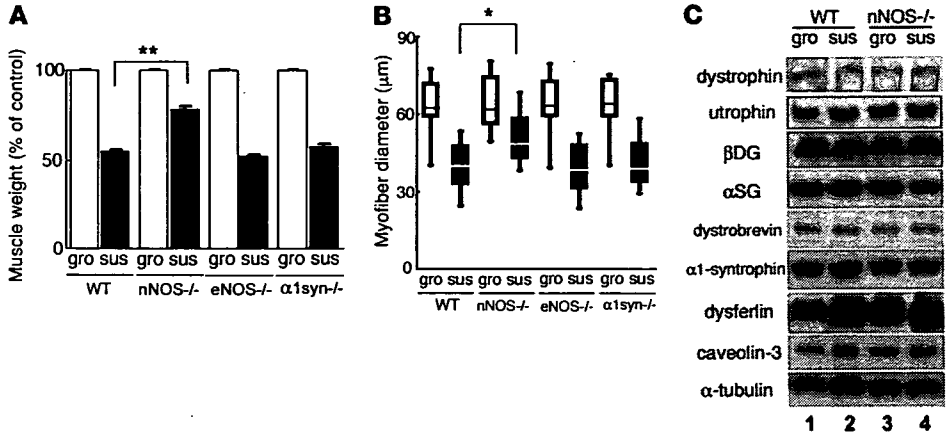

Figure 2

nNOS-null mice show partial tolerance to disuse-induced muscle atrophy. **(A)** Soleus muscle weight from ground control and tail-suspended wild-type ($n = 20$), nNOS-null ($n = 20$), eNOS-null ($n = 10$), and α1-syntrophin–null ($n = 10$) mice after 2-week tail suspension is shown as percent of wild-type ground controls. $^{**}P < 0.01$, Student's t test. **(B)** Box and whiskers plot of diameter of myofiber in soleus. Diameters were measured on H&E-stained cross sections of soleus muscles. $n = 200$ fibers in each experiment. $^{*}P < 0.05$, Student's t test. **(C)** Immunoblots of mouse gastrocnemius muscle extracts for DGC components from wild-type ground control (lane 1), wild-type tail-suspended (lane 2), nNOS-null ground control (lane 3), and nNOS-null tail-suspended (lane 4) mice. All lanes contain 30 μg of total protein. The experiments were performed 5 times, and representative pictures are presented.

(Figure 1C). eNOS expression was not changed (Figure 1D), and iNOS was not expressed (data not shown) during the course.

Next we performed subcellular fractionation of muscle homogenates as described previously (24). In ground control mice, nNOS remained in the insoluble pellet (Figure 1D). In tail-suspended mice, nNOS was largely extracted with 100 mM NaCl and barely detected in the pellet fraction (Figure 1D). Quantification of nNOS bands clearly showed that nNOS dislocated from the sarcolemma to the cytoplasm during tail suspension (Figure 1E). These results indicate that nNOS exists mainly in the cytoplasm during tail suspension. Immunoprecipitation experiments also revealed that nNOS completely dissociated from α1-syntrophin and caveolin-3 during tail suspension (Figure 1, G and H). In contrast, a considerable amount of dysferlin was immunoprecipitated with nNOS antibody during tail suspension (Figure 1I).

nNOS-null mice represent tolerance to disuse-induced muscle atrophy. To examine the roles of dislocated nNOS in muscle atrophy, we then performed tail suspension experiments using wild-type, nNOS-null, eNOS-null, and α1-syntrophin–null mice. The body weight (Figure 2A), average muscle fiber diameter (Figure 2B), and total number of muscle fibers (data not shown) of nNOS-null mice in the ground condition were similar to those of wild-type mice. However, after tail suspension for 14 days, reduction of muscle weight (Figure 2A), muscle size (Figure 2B), and muscle power (Supplemental Figure 1) were significantly less severe in the nNOS-null mice. Except for nNOS, dystrophin and other components of DGC were expressed in nNOS-null muscle at the same level as in wild-type muscle in both ground and suspended conditions (Figure 2C). eNOS-null muscle revealed atrophy during tail suspension similar to that seen in wild-type muscle (Figure 2, A and B), indicating that eNOS is not essential for atrophy signaling. We previously reported that disruption of the α1-syntrophin gene resulted in dislocation of nNOS from the sarcolemma to the cytoplasm without dystrophic phenotypes (25, 26). Suspension of α1-syntrophin–null mice induced severe muscle atrophy as it did in wild-type muscle (Figure 2, A and B).

Production of NO by nNOS in tail-suspended skeletal muscle. To directly measure the levels of NO in skeletal muscle during tail suspension, we employed electron paramagnetic resonance (EPR) spectrometry with *N*-methyl-D-glucamine-dithiocarbamate (MGD) and Fe^{2+} (27, 28). We injected MGD and Fe^{2+} into the wild-type and nNOS-null mice at the final stage of 2-week suspension, sacrificed the mice 30 minutes after the injection, and immediately measured the NO levels in muscle tissues. In EPR, the signal height, which is proportional to the amount of NO, was obtained by measuring the peak-to-peak height of the lower field side signal (arrow in Figure 3A) in the characteristic 3-line NO spectrum (29). NO levels in skeletal muscles increased during tail suspension, and the increase was inhibited by daily administration of 7NI to the mice. We used 50 mg/kg of 7NI to selectively inhibit nNOS (30, 31). The increase of NO levels in skeletal muscle during tail suspension was also inhibited by daily administration of 10 mg/kg of N-nitro-L-arginine methylester (L-NAME; pan-NOS inhibitor) (30) to the same extent (data not shown). NO levels in the skeletal muscle of nNOS-null mice after tail suspension were not different from those of ground control mice (Figure 3B), indicating that nNOS is mainly responsible for elevated levels of NO in muscle during tail suspension. Assay of the catalytic activity of NOS showed a higher level in the soluble (cytoplasmic) fraction than in the particulate fraction of suspended wild-type mice (Figure 3C).

Production of NO by nNOS is upstream of Foxo3a pathway. Foxo transcription factors are reported to upregulate many atrophy-related genes and promote muscle atrophy (9, 10). We found that Foxo3a was dephosphorylated and accumulated in the myonuclei of wild-type mice but not nNOS-null mice in western blotting (Figure 4, A and B) and in immunohistochemistry (Supplemental Figure 3). Foxo1 and Foxo4 were not changed during tail suspension in both wild-type and nNOS-null mice (Figure 4B). Recently, several groups have pointed out that the ubiquitin proteasome pathway is largely involved in selective protein degradation during the muscle atrophy process (3, 4). Consistent with this, mRNA levels of 2 muscle-specific E3 ubiquitin ligases, MuRF-1 and atrogin-1/MAFbx, increased during tail suspension in wild-type mice (Figure 4C) (9, 10). Remarkably, the upregulation of these E3 ligases was modest in nNOS-null mice. These observations suggest that nNOS regulates Foxo3a via NO production and thereby upregulates MuRF-1 and atrogin-1/MAFbx. To further examine whether nNOS regulates Foxo3a, we overexpressed nNOS in myotubes by a retrovirus vector (Supplemental Figure 4). Overexpressed nNOS increased both total and nuclear Foxo3a protein levels and decreased phosphorylated Foxo3a in myotubes (Supplemental Figure 4).

NF-κB pathway is activated during muscle atrophy in nNOS-null mice. NF-κB has been shown to be a major regulator of tail suspension–induced

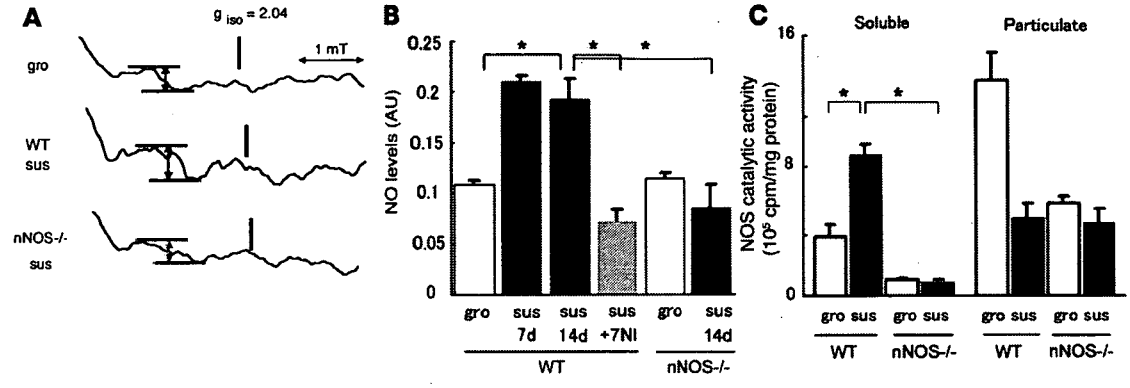

Figure 3

Measurement of NO in muscle and NOS activity during tail suspension. (**A**) EPR spectra of the NO adduct of Fe-MGD complex observed in skeletal muscle at room temperature. The NO-trapping agent was injected 30 minutes before measurements were taken. The EPR spectra of ground control and tail-suspended wild-type and nNOS-null mice were shown. Each spectrum represents the average of 5 accumulations. The signal height was obtained by measuring the peak-to-peak height of the lower field side signal (vertical arrows) in the 3-line spectrum. (**B**) NO levels of the skeletal muscle with and without tail suspension for 7 or 14 days were analyzed in EPR spectrometry ($n = 6$; $^*P < 0.05$, Mann-Whitney). Note that NO level in muscle is elevated in wild-type tail-suspended mice at 14 days but not in nNOS-null tail-suspended mice. 7NI was used as a selective nNOS inhibitor. (**C**) NOS catalytic activity in soluble and particulate fractions ($n = 5$; Mann-Whitney). [^{3}H]-citrulline, converted from [^{3}H]-arginine in vitro by NOS, was quantified by liquid scintillation spectroscopy. Note higher NOS activities in the soluble fraction than in the particulate fraction for suspended wild-type mice.

muscle atrophy (20, 21). EMSA showed that binding activity of NF-κB to its authentic binding sequence is increased by tail suspension in both wild-type and nNOS-null mice (Figure 4D). Importantly, there was no difference between tail-suspended wild-type and nNOS-null mice in the NF-κB binding activity (Figure 4D). In addition, western blotting revealed that p50 is increased by tail suspension (data not shown). These results suggest that NF-κB pathway was activated during tail suspension in the absence of nNOS. Whether the NF-κB activities mediate the residual muscle atrophy that occurred in nNOS-null mice during tail suspension remains to be clarified in a future study.

Inhibitor of NF-κB kinase β is nitrosylated during tail-suspension. Foxo3a is known to be phosphorylated by Akt in skeletal muscle (10, 18). In contrast to our expectation, there was no difference between wild-type and nNOS-null mice in the phosphorylation levels of Akt (Figure 5, A and B). There was no difference between the levels of S6k1 and mammalian target of rapamycin (mTOR), which are under regulation by PI3K/Akt signaling and positively regulate protein synthesis between wild-type and nNOS-null mice during tail suspension (5) (Figure 5A). A recent study reported that NO S-nitrosylates inhibitor of NF-κB kinase β (IKKβ) and thereby inhibits its activity (32). Other reports described inhibition of Foxo3a by IKKβ (33). Intriguingly, we found that tyrosine residues of IKKβ were nitrosylated during tail suspension in wild-type mice but not in nNOS-null mice (Figure 5C). However, whether S-nitrosylation of IKKβ detected during tail suspension contributes to activation of Foxo3a remains to be determined.

7NI alleviates tail suspension–induced muscle atrophy. To further examine the effect of inhibition of nNOS activity on muscle atrophy, 7NI, a nNOS-selective inhibitor, was injected daily into the peritoneal space of the wild-type mice during the 2-week tail suspension (Figure 6). This treatment significantly prevented muscle atrophy during tail suspension but did not increase muscle mass of ground control mice (Figure 6A). 7NI considerably increased phosphorylated Foxo3a and inhibited the increase in dephosphorylated and nuclear Foxo3a during tail suspension (Figure 6C). We also found that upregulation in mRNA levels of MuRF-1 and atrogin-1/MAFbx was abolished by 7NI during tail suspension (Figure 6B). These data imply that nNOS-specific inhibitor is a potential therapeutic strategy for disuse-induced muscle atrophy.

nNOS-null mice show milder muscle atrophy than wild-type mice after cutting of the sciatic nerve. We next examined the role of nNOS in denervation-induced muscle atrophy. Cutting the sciatic nerve on the denervated side resulted in greatly reduced muscle weight 14 days after operation (Figure 7A). Importantly, nNOS had already disappeared from the sarcolemma 3 days after denervation (Figure 7A). We observed much milder muscle atrophy in denervated muscle of nNOS-null mice than wild-type mice (Figure 7B), suggesting that nNOS is also involved in denervation-induced muscle atrophy. We then tested whether an nNOS inhibitor (7NI) or a pan-NOS inhibitor (L-NAME) counteracts denervation-induced muscle atrophy (Figure 7B). These 2 inhibitors limited the muscle atrophy (Figure 7B), indicating that NO is indeed a mediator and therefore a therapeutic target for denervation-induced muscle atrophy.

Discussion

Dislocation of nNOS is a major step in tail suspension–induced muscle atrophy. Involvement of the DGC in cachexia-induced muscle atrophy was recently reported (22). In our report, we demonstrate for what we believe to be the first time that nNOS is dislocated from the sarcolemma to the cytoplasm during tail suspension, whereas other members of the DGC are normally expressed at the sarcolemma. This observation implies that different mechanisms are involved in unloading-induced muscle atrophy and muscle atrophy seen in cachexia. Sarcolemmal nNOS is reported to be a versatile molecule that modulates satellite cell activation (34), formation of neuromuscular junction (35), glucose uptake (36), muscle contraction, and vasodilation (37). To clarify the mechanisms of nNOS translocation, we examined the effects of clenbuterol, streptomycin, and nifedipine on nNOS dislocation during tail suspension. After administration of these drugs, however, we still observed dislocation of nNOS during tail suspension (data not shown). These results suggest that sympathetic nerves, stretch-activated chan-

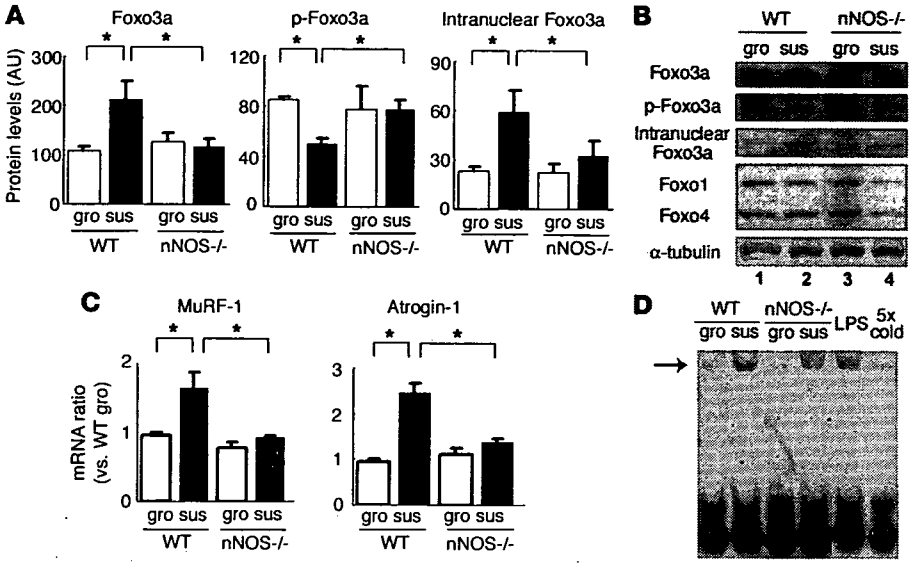

Figure 4

Participation of nNOS in regulation of Foxo3a and upregulation of MuRF-1 and atrogin-1/MAFbx. **(A)** The amounts of total Foxo3a, phosphorylated Foxo3a (p-Foxo3a), and intranuclear Foxo3a in wild-type and nNOS-null muscle during tail suspension were quantified (n = 5). Note that Foxo3a was dephosphorylated and accumulated in the myonuclei of wild-type mice but not of nNOS-null mice. *P < 0.05, Mann-Whitney. **(B)** Representative immunoblot analysis for Foxo3a, phosphorylated Foxo3a, Foxo1, and Foxo4 in total muscle extract, and Foxo3a in nuclear extracts in wild-type ground control (lane 1), wild-type tail-suspended (lane 2), nNOS-null ground control (lane 3), and nNOS-null tail-suspended (lane 4) muscles. α-Tubulin was used as a loading control. **(C)** mRNA levels of ubiquitin ligases (MuRF-1 and atrogin-1/MAFbx) (n = 5) were quantified by real-time RT-PCR. *P < 0.05, Mann-Whitney. **(D)** EMSA of NF-κB. Biotin-labeled double-stranded oligonucleotides containing NF-κB binding sites were incubated with nuclear extracts prepared from ground control and suspended muscles. An arrow indicates the DNA-protein complex. LPS was injected intraperitoneally into mice, and the muscle was used as a positive control for NF-κB binding activity. 5× cold, 5-fold excess of nonlabeled competitors.

nels, and L-type calcium channels are not involved in the dissociation of nNOS from the DGC.

nNOS is anchored at the sarcolemma by interaction with α1-syntrophin (25), a member of the DGC; interestingly, however, α1-syntrophin remains at the sarcolemma during tail suspension (data not shown). To examine whether modification of α1-syntrophin is involved in the dissociation of nNOS from α1-syntrophin, we performed 2-dimensional PAGE and western blotting with anti-α1-syntrophin antibody as previously described (38). The first dimensional isoelectric focusing reveals posttranslational modifications of α1-syntrophin. The results showed slight changes in mobility pattern of α1-syntrophin during tail suspension (data not shown), suggesting that some posttranslational modifications of α1-syntrophin may cause dissociation of nNOS from α1-syntrophin.

Dislocated nNOS leads to production of NO and regulates Foxo/E3 ubiquitin ligases pathway. EPR spectrometry confirmed that cytoplasmic nNOS led to production of NO during tail suspension (Figure 3, A and B). Tail suspension–induced muscle atrophy was blunted in nNOS-null mice (Figure 2, A and B) and 7NI-treated mice (Figure 6A) but not in eNOS-null mice (Figure 2, A and B). iNOS protein was not detected by western blotting in skeletal muscle during tail suspension (data not shown). These data indicate that dislocated nNOS, but neither eNOS nor iNOS, is involved in tail suspension–induced muscle atrophy.

We clearly show that 2 atrophy-related E3 ubiquitin ligases, MuRF-1 and atrogin-1/MAFbx, are not upregulated in nNOS-null muscle during tail suspension (Figure 4C and Figure 6B). Therefore, the induction of these genes is a downstream event of dislocation of nNOS in tail suspension–induced muscle atrophy.

Foxo transcription factors are reported to induce skeletal muscle atrophy by upregulating MuRF-1 or atrogin-1/MAFbx (4, 10, 16, 17). For example, transgenic mice overexpressing Foxo1 in skeletal muscle display a decrease in size of muscle fibers (17). Importantly, Foxo3a remained phosphorylated in nNOS-null mice during tail suspension, and total Foxo3a protein was not increased in tail-suspended nNOS null mice. Moreover, Foxo3a accumulated in the myonuclei of wild-type but not in nNOS-null mice during tail suspension (Figure 4B and Figure 6C).

When we overexpressed nNOS in muscle cells using a retrovirus vector, we found that Foxo3a was activated in nNOS-overexpressing myotubes (Supplemental Figure 4).

How does nNOS/NO regulate Foxo3a pathways? Our observations suggest that nNOS/NO is an upstream regulator of Foxo3a in the tail suspension–induced muscle atrophy process. There are at least 2 possible explanations for how Foxo3a regulates nNOS/NO. First, NO produced by nNOS might inhibit protein kinases, which phosphorylate Foxo3a, thereby protecting Foxo3a from degradation and promoting its translocation from the cytoplasm to the nucleus. There are several kinases that can phosphorylate Foxo, including Akt (10), IKKβ (33), BCR (39), and CDK2 (40). In the present study, we show that Akt activities in nNOS-null muscle were not different from those in wild-type muscle during tail suspension. A fraction of IKKβ was nitrosylated (inactivated) during tail suspension (Figure 5C), but NF-κB was activated in both wild-type and nNOS-null muscle during suspension. This observation suggests that IKKβ activity was not meaningfully disrupted (Figure 4D). Involvement of other kinases remains to be investigated in a future study.

Second, nNOS/NO signal might decrease nuclear export of Foxo3a, resulting in accumulation of Foxo3a in myonuclei and protecting it from phosphorylation by Akt. Foxo is exported from the nucleus in a 14-3-3 protein–dependent process (19), and these molecular interactions remain to be examined.

Dislocation of nNOS and production of NO have no obvious effects on the activity of NF-κB. It has been reported that reduced muscle activity induces muscle atrophy via activation of both Foxo and NF-κB transcription factors (9), at the same time suppressing the Akt pathway (5, 6), resulting in activation of the transcription of MuRF-1 and atrogin-1/MAFbx genes. In this report we demonstrated that dephosphorylation and nuclear accumulation of Foxo3a were largely attenuated in nNOS-null muscle during tail suspension. In contrast, our EMSA assay suggested that the NF-κB pathway was activated in nNOS-null

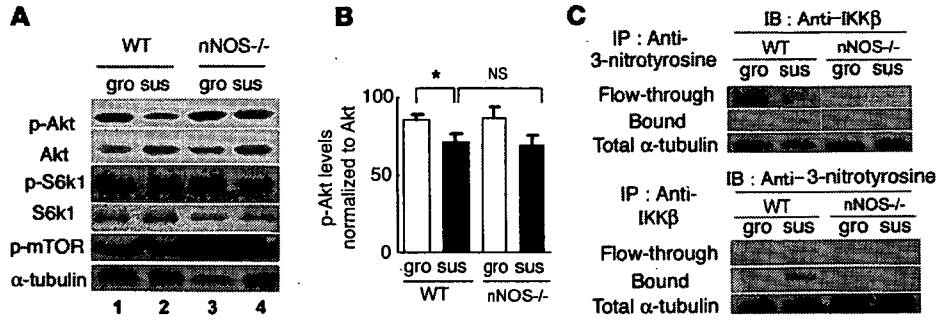

Figure 5

Phosphorylation of Akt and nitrosylation of IKKβ during 2-week tail suspension. (**A**) Immunoblots for protein synthesis pathway components (p-Akt, Akt, p-S6k1, S6k1, and p-mTOR) in wild-type ground control (lane 1), wild-type tail-suspended (lane 2), nNOS-null ground control (lane 3), and nNOS-null tail-suspended (lane 4) muscles. Densities of the bands were normalized to α-tubulin. (**B**) The ratio of phosphorylated Akt to total Akt is shown ($n = 5$; $^*P < 0.05$, Mann-Whitney). (**C**) Detection of nitrosylated IKKβ. Muscle proteins were immunoprecipitated with anti–3-nitrotyrosine antibody (upper panel) or with anti-IKKβ antibody (lower panel) and immunoblotted with anti-IKKβ or anti–3-nitrotyrosine antibodies, respectively. α-Tubulin signals in flow-through fractions are also shown.

mice to a similar extent as in wild-type mice in tail suspension experiments. This observation raises the possibility that NF-κB mediated the residual atrophy that occurred in nNOS-null mice, but further investigation is needed to correctly answer this question.

nNOS and other muscle atrophies. Many conditions induce muscle atrophy, including space flight, immobilization, denervation, cancer cachexia, motor neuron diseases, starvation, and aging (41). Recently it has been reported that muscles of tumor-bearing mice exhibited membrane abnormalities accompanied by reduced levels of dystrophin and increased glycosylation on DGC proteins (22, 23). It was also shown that the DGC could counteract atrophic signaling in cancer cachexia when overexpressed at the sarcolemma (22). In the tail suspension model, we observed dislocation of nNOS but no changes in the sarcolemmal expression of other members of the DGC (Figure 2C). Therefore it is possible that dystrophin deficiency in cancer cachexia induces nNOS dislocation, which results in activation of nNOS and its downstream effectors.

We also found nNOS dislocation in denervation-induced muscle atrophy (Figure 7A). Remarkably, denervation-induced muscle atrophy was modestly blunted in nNOS-null mice or selective nNOS inhibitor–treated mice (Figure 7B). Although iNOS was induced during denervation (data not shown), both 7NI and L-NAME showed a similar effect on muscle atrophy, suggesting that iNOS does not contribute to denervation-induced muscle atrophy.

In conclusion, we demonstrate that nNOS dislocated from the sarcolemma to the cytoplasm in 2 models of disuse-induced muscle atrophy, tail suspension and denervation. We also show that dislocated nNOS led to the production of NO and regulated Foxo3a, MuRF-1, and atrogin-1/MAFbx, key molecules in muscle atrophy. Our model is illustrated in Figure 8. The identification of nNOS as a regulator of unloading-induced muscle wasting suggests that pharmacological intervention targeting nNOS or its downstream or upstream pathways would prevent or diminish this debilitating process.

Methods

Animals and tail suspension model. Twelve-week-old female C57BL/6, nNOS-null and eNOS-null mice were purchased from the Jackson Laboratory. α1-Syntrophin-null mice were produced in our previous study (25). These mice were backcrossed to the C57BL/6 strain for more than 10 generations. The animals were allowed ad libitum access to food and drinking water. The Experimental Animal Care and Use Committee of the National Institute of Neuroscience approved all experimental protocols. The mice were randomly assigned to control or tail suspension groups. To induce muscle atrophy by disuse, mice were suspended so that their hind limbs were 1 mm off the cage floor for 14 days. After 14 days of tail suspension, some groups were allowed 7 days of reloading by normal weight bearing. Muscle weight was normalized to body weight and is presented as a percentage of control in each experiment.

Denervation model. The left sciatic nerve of mice was excised for nearly the full length of the thigh (approximately 10 mm) from a small incision (approximately 4 mm) made in the mid-lateral thigh under general anesthesia under a surgical microscope (Olympus) (42). The mice were sacrificed 3 or 14 days after denervation by cervical dislocation under general anesthesia, and soleus and gastrocnemius muscles were excised for analysis. The right gastrocnemius muscle served as a control.

Reagents. Lipopolysaccharide from *E. coli* (0.1 ml, 3 mg/kg; *E. coli*, serotype 055:B5; Sigma-Aldrich) was administered via intraperitoneal injection. 7NI (Dojindo) was dissolved in peanut oil (50 mg/kg). L-NAME was injected daily into the intraperitoneal cavity of mice (10 mg/kg body weight). Clenbuterol (1 mg/kg; Sigma-Aldrich), streptomycin (300 mg/kg; Sigma-Aldrich) and nifedipine (5 mg/kg; Wako) were dissolved in PBS. PBS was injected into control mice.

Tissue preparation. Control and tail-suspended mice were sacrificed with cervical dislocation. Body and wet muscle were weighed. The gastrocnemius and soleus muscles were collected individually using standard dissection methods and cleaned of excess fat, connective tissue, and tendons. Several of the muscles were frozen in isopentane cooled by liquid nitrogen for histological and immunohistochemical analysis, and the other muscles were frozen directly in liquid nitrogen for RNA isolation or protein extraction and stored at -80°C.

Real time PCR. Total RNA was isolated using TRIzol (GIBCO). For RT-PCR, first-strand cDNA was synthesized using oligo-dT primers. Expression levels of selected genes (nNOS, MuRF-1, atrogin-1/MAFbx, and 18S-rRNA) were analyzed using Applied Biosystems SYBR Green gene expression assays on ABI7700 Sequence Detection System (Applied Biosystems) following the manufacturer's instructions.

H&E staining. Ten-micrometer cryosections were cut in the middle part of the muscle belly to obtain the largest myofiber diameter, placed on poly-L-lysine–coated slides, air dried, and stained with H&E. The sections were viewed and photographed using an HC-2500 digital camera system (Fuji Photo Film).

Immunohistochemistry. Cryostat sections of muscle tissue (10 μm thick), were postfixed in acetone or 4% paraformaldehyde at -20°C and preincubated in PBS containing 5% goat serum and 1% bovine serum albumin for 30 minutes at room temperature. Polyclonal anti-nNOS (Zymed), anti-Foxo3a (Sigma-Aldrich), and anti-laminin-α2 (Alexis) were applied overnight at 4°C. Following incubations with appropriate secondary antibodies, mounted sections were observed by using a Leica confocal microscope. Muscle fiber diameters were determined on cross sections of soleus muscle using the greatest distance between the oppo-

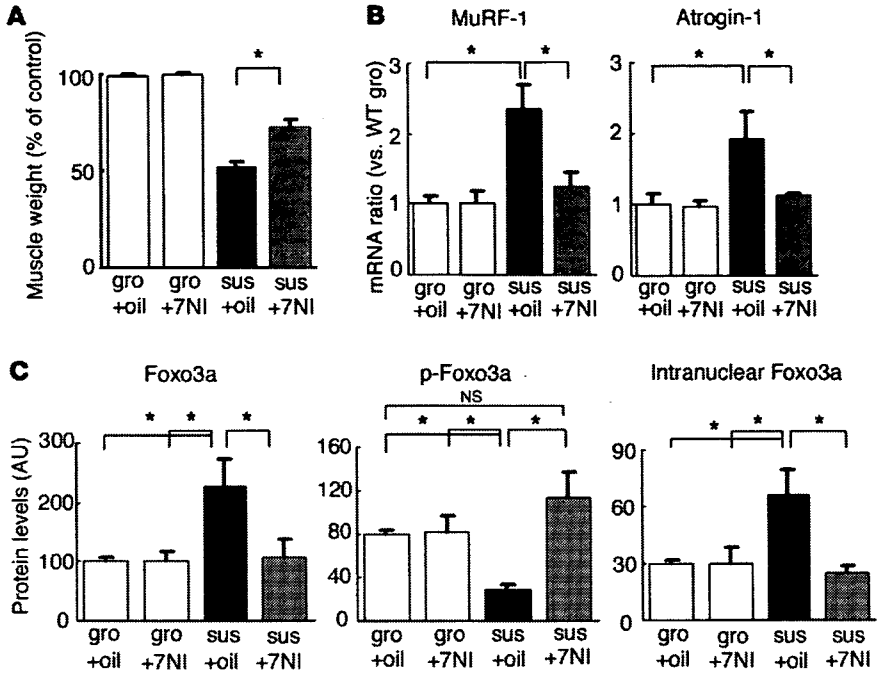

Figure 6
7NI alleviates muscle atrophy during tail suspension. (**A**) Soleus muscle weight of wild-type ground control and wild-type tail-suspended mice with (+7NI) or without 7NI (+oil). Oil or 7NI (50 mg/kg/d) was injected daily into the abdominal cavity of the mice during 2-week tail suspension. Values (muscle weight/body weight) are expressed as percent of wild-type oil-injected muscles after 14-day tail suspension (n = 5–10 per group; $^*P < 0.05$, Mann-Whitney). (**B**) mRNA levels of MuRF-1 and atrogin-1/MAFbx (n = 4) in muscle from wild-type ground control and wild-type tail-suspended mice with or without 7NI were quantified by real-time RT-PCR ($^*P < 0.05$, Mann-Whitney). (**C**) The amount of total Foxo3a, dephosphorylated Foxo3a, and intranuclear Foxo3a (n = 4) were analyzed by western blotting, and band densities were normalized to α-tubulin ($^*P < 0.05$, Mann-Whitney).

site sides of the narrowest aspect of the fiber. Total number of muscle fibers was also counted on cross sections.

Western blotting. Total skeletal muscle protein was extracted from mouse hindlimb muscle for western blot analysis. We used the Bradford method and Coomassie Brilliant Blue G-250 (Bio-Rad) to determine the protein concentrations. Then protein fractions were extracted with a reducing sample buffer containing 10% SDS, 70 mM Tris-HCl, 5% β-mercaptoethanol, and Complete inhibitor cocktail (Roche). Protein (15 or 30 μg per lane) was separated on an SDS-polyacrylamide gel. The resulting gel was subsequently transferred to a polyvinylidene difluoride membrane (Millipore) using 242 mA for 1 hour. The blot was later incubated with primary antibodies. The signals were detected using the enhanced chemiluminescence method (GE Amersham). Relative quantities of proteins in western blots were determined by scanning densitometry (Alpha Innotec) and expressed in arbitrary units. The following antibodies were used for immunoblotting: anti-α1-syntrophin (Biogenesis), anti-laminin-α2 (Alexis), anti-dystrophin (dys2), anti-utrophin, anti-β-dystroglycan, anti-dystrobrevin, anti-dysferlin, anti-caveolin-3 (Novocastra), anti-hsp90 (Stressgen), anti-nNOS, anti-IKKβ, anti-Akt, anti-p-Akt, anti-p-mTOR, anti-p50 (Transduction Laboratories), anti-Foxo3a, anti-p-Foxo3a, anti-Foxo1/4, anti-Na/K-ATPase (Upstate Biotechnology), anti-Hsp70, and anti-iNOS antibody (Santa Cruz Biotechnology Inc.). Anti-α-sarcoglycan antibody was kindly provided by Michihiro Imamura (National Institute of Neuroscience, National Center of Neurology and Psychiatry).

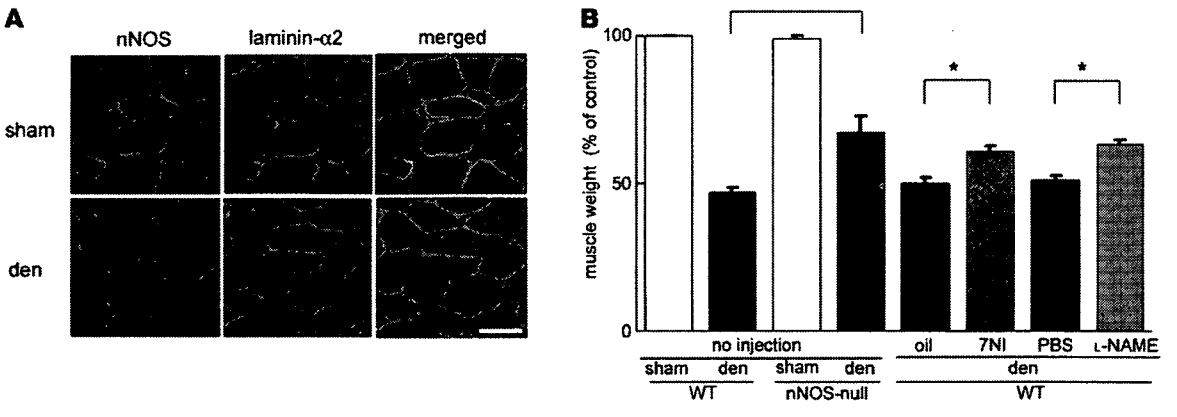

Figure 7
Inhibition of nNOS activities counteracts denervation-induced muscle atrophy. (**A**) Sarcolemmal expression of nNOS in control and denervated muscles. Transverse muscle sections from denervated (den) and sham-operated mice were stained with anti-nNOS (green) and anti-laminin-α2 chain (red) antibodies 3 days after sciatic nerve excision. Scale bar: 50 μm. (**B**) Reduction in soleus muscle weight of wild-type and nNOS-null mice 2 weeks after sham operation or denervation. Weight of wild-type denervated muscle was also measured after 2-week administration of oil, 7NI, PBS, or L-NAME. Values (muscle weight/body weight) were expressed as percentage of the values of sham-operated wild-type muscles (n = 5–10 per group). $^*P < 0.05$, Mann-Whitney.

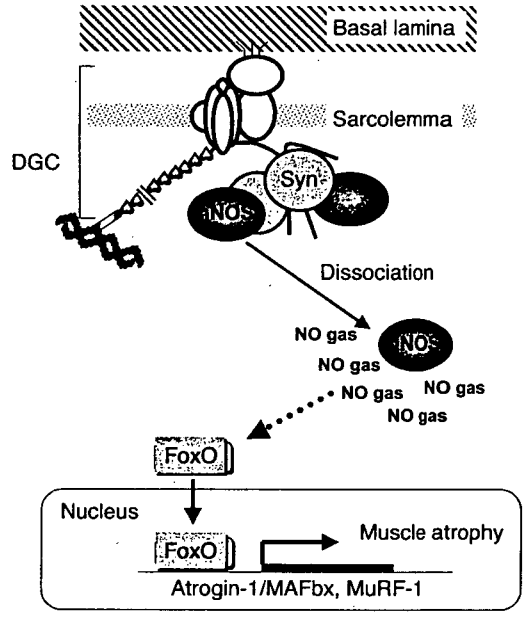

Figure 8
A model of nNOS involvement in tail suspension–induced muscle atrophy. Under normal conditions nNOS is located at the sarcolemma as a peripheral member of the DGC. During tail suspension, nNOS dissociates from α1-sytrophin (syn) and dislocates into the cytoplasm, generating NO, which ultimately regulates Foxo transcription factors, and muscle-specific E3 ubiquitin ligases, MuRF-1, and atrogin-1/MAFbx, which promote muscle protein degradation by the ubiquitin-proteasome system.

Nuclear and cytosolic protein extraction. Nuclear extracts were prepared from mouse skeletal muscle according to the method of Hunter et al. (20). Briefly, the cytosolic extract was obtained from the first supernatant of the nuclear extract preparation. The supernatant was placed in Millipore Ultrafree-4 centrifugal columns that had been pre-wetted with 0.5 ml of dilution buffer (20 mM HEPES, 40 mM KCl, 10% glycerol, 0.2 mM EDTA, 1 mM DTT), and centrifuged (7,500 *g*) at 4°C for 30 minutes. Dilution buffer (0.8 ml) was added to the column, and the 30-minute spin was repeated. Protein concentrations were determined using the Bradford protein assay (Bio-Rad).

Immunoprecipitation. Skeletal muscle samples were homogenized in 0.15 M NaCl, 10 mM HEPES (pH 7.5) and Complete inhibitor cocktail (Roche), with or without 1% digitonin (Wako). nNOS and caveolin-3 immunoprecipitation was performed with anti-nNOS goat polyclonal antibody (Santa Cruz Biotechnology Inc.) and anti-caveolin-3 antibody (Transduction Laboratories). The samples were incubated with protein G gel (GE Amersham) overnight at 4°C. After the gel was washed with the equilibrating buffer, the bound fraction was eluted with 1% SDS, 1 mM tris-(2-carboxyethyl) phosphine, and 14 mM Tris-HCl (pH 6.7) and concentrated. Coimmunoprecipitates were resolved by SDS-PAGE and analyzed by western blotting. α-Tubulin was used as internal control for total protein inputted.

Two-dimensional PAGE. Muscle extracts from ground control and tail suspension mice were resolved on 2-dimensional PAGE and analyzed by western blotting as described in ref. 38.

EMSA. EMSA was performed according to the manufacturer's instructions (Panomics). Briefly, probes were end-labeled with biotin. Binding reactions were performed for 30 minutes in a volume of 10 ml. Specificity of DNA binding was determined by addition of a 5-fold molar excess of unlabeled competitor DNA to the binding reactions. The binding reactions were loaded onto 6% non-denaturing polyacrylamide gels and electrophoretically resolved in 0.5× tris-borate EDTA (TBE) buffer.

NOS catalytic assays. NOS catalytic assays were carried out according to the method described by Brenman et al. (24). Muscles from wild-type and nNOS-null mice with or without tail suspension were homogenized in 10 volumes of buffer containing 25 mM Tris-HCl, pH 7.4, 1 mM EDTA, 1 mM EGTA, and 0.1 mM NaCl. The homogenate was centrifuged at 20,000 *g* to separate the soluble fraction. The pellet was extracted in the same buffer containing 0.5 M NaCl and centrifuged at 20,000 *g* to create a particulate fraction. Aliquots from these fractions were assayed in 125-μl reactions containing 1.8×10^5 cpm of [^{3}H]-arginine (53.0 Ci/mmol; GE Amersham), 1 mM NADPH, 640 μM $CaCl_2$, 1 μM calmodulin, and 3 μM each of tetrahydrobiopterin, FAD, and FMN. After incubation for 20 minutes at 37°C, the assays were terminated with 2 ml of 20 mM HEPES, pH 5.5, and 2 mM EDTA. The samples were then applied to AG50WX-8 columns (Na^+ form; Dowex), which were centrifuged, and the supernatant was collected. [^{3}H]-citrulline was quantified by liquid scintillation spectroscopy.

Subcellular fractionation. The subcellular fractionation was performed according to the method described by Brenman et al. (24). The gastrocnemius muscle was homogenized in 10 volumes (w/v) of buffer A (25 mM Tris-HCl, pH 7.4, 100 mM NaCl, 1 mM EDTA, 1 mM EGTA). The nuclei of the muscle were pelleted by centrifugation at 1,000 *g*. The supernatant was then centrifuged at 20,000 *g* to yield the supernatant S1. The resulting heavy microsomal pellet was resuspended in buffer B (500 mM NaCl added to buffer A), incubated for 30 minutes at 4°C with agitation, and centrifuged at 15,000 *g*, yielding supernatant S2. The pellet from this last centrifugation was resuspended in buffer B containing 0.5% Triton X-100, incubated for 30 minutes at 4°C with agitation, and centrifuged at 15,000 *g* to create supernatant S3 and the final pellet. The fractions were resolved using the sample buffer and analyzed by SDS-polyacrylamide gel electrophoresis. The proteins were transferred to a polyvinylidene difluoride membrane (Millipore), which was later incubated with anti-nNOS antibody. The bands were quantified in densitometry.

Direct measurement of NO by EPR spectrometry. Concentrations of NO in the skeletal muscle of mice were measured using the NO-trapping technique combined with EPR spectroscopy (29). Spin traps react with unstable free radicals such as NO to form a relatively stable radical adduct. This long-lived adduct formation results in accumulation of a steady-state formation of these free radicals, and thus the resultant radical adduct can be detected readily by EPR spectroscopy. We used a Fe-MGD complex as the trapping agent to quantify NO levels in the skeletal muscle tissues of the mice. Solutions of $FeSO_4$ (62 mg/kg; Wako) and MGD (348 mg/kg; Dojindo) were injected subcutaneously. The Fe-MGD complex formed had a high specificity for NO (27, 29), and the NO-Fe-MGD complex was detected by EPR spectroscopy. The amplitude of the signal measured from the peak-to-peak height of the lower field side signal in the 3-line spectrum is known to be proportional to the amount of NO (29). The level of NO-Fe-MGD complex was estimated by comparing it with the signal height of a standard solution of a chemically synthesized NO complex. The concentration in tissues was determined 30 minutes after injection of the NO-trapping reagent. Thirty minutes after administration of the reagent, the gastrocnemius and soleus muscle were removed and weighed (approximately 100–120 mg). The tissue was minced and subjected to immediate measurement of NO by EPR spectrometry. X-band EPR spectra were measured at room temperature with a TE-200 EPR spectrometer (JEOL). The homogenates were drawn into a capillary tube (75 mm in length, 46 μl in internal volume) that had been inserted first into an EPR quartz tube (outside diameter, 5 mm), then introduced into the cavity. The instrument settings were as follows: center field, 331 mT; field scan, 4 mT; sweep time, 2 min; time

constant, 0.3 s; modulation amplitude, 0.32 mT; modulation frequency, 9.44 GHz; microwave power, 60 mW.

Statistics. Statistical differences were determined by either 2-tailed unpaired Student's *t* test or the Mann-Whitney test. All data are expressed as mean ± SEM. Statistical significance is defined as $P < 0.05$.

Acknowledgments

We thank S. Masuda, A. Fukase, and T. Harano for technical support; K. Asanuma and J. Yoshitake for EPR spectrometry; Y. Onodera and M. Tateyama for immunohistochemistry; and all members of the Department of Molecular Therapy, National Institute of Neuroscience, for technical assistance and useful discussion, especially M. Yoshida, M. Ikemoto, and Y. Mochizuki. We also thank K. Ono for correcting our English. This work was supported by Research on Nervous and Mental Disorders (grant 16B-2); Health Science Research Grants for research on the human genome and gene therapy (H16-genome-003) and for research on brain science (H15-kokoro-021 and H18-kokoro-019) from the Japanese Ministry of Health, Labor and Welfare; Grants-in-Aid for Scientific Research (14657158, 15390281, 16590333, 17590857, and 18590392) from the Japanese Ministry of Education, Culture, Sports, Science and Technology; and the Ground-based Research Program for Space Utilization, promoted by Japan Space Forum.

Received for publication October 16, 2006, and accepted in revised form May 29, 2007.

Address correspondence to: Shin'ichi Takeda, Department of Molecular Therapy, National Institute of Neuroscience, National Center of Neurology and Psychiatry, 4-1-1 Ogawa-higashi, Kodaira, Tokyo 187-8502, Japan. Phone: 81-42-346-1720; Fax: 81-42-346-1750; E-mail: takeda@ncnp.go.jp.

1. Tidball, J.G. 2005. Mechanical signal transduction in skeletal muscle growth and adaptation. *J. Appl. Physiol.* **98**:1900–1908.
2. Ikemoto, M., et al. 2001. Space shuttle flight (STS-90) enhances degradation of rat myosin heavy chain in association with activation of ubiquitin-proteasome pathway. *FASEB J.* **15**:1279–1281.
3. Bodine, S.C., et al. 2001. Identification of ubiquitin ligases required for skeletal muscle atrophy. *Science.* **294**:1704–1708.
4. Gomes, M.D., Lecker, S.H., Jagoe, R.T., Navon, A., and Goldberg, A.L. 2001. Atrogin-1, a muscle-specific F-box protein highly expressed during muscle atrophy. *Proc. Natl. Acad. Sci. U. S. A.* **98**:14440–14445.
5. Bodine, S.C., et al. 2001. Akt/mTOR pathway is a crucial regulator of skeletal muscle hypertrophy and can prevent muscle atrophy in vivo. *Nat. Cell Biol.* **3**:1014–1019.
6. Song, Y.H., et al. 2005. Muscle-specific expression of IGF-1 blocks angiotensin II-induced skeletal muscle wasting. *J. Clin. Invest.* **115**:451–458. doi:10.1172/JCI200522324.
7. Rommel, C., et al. 2001. Mediation of IGF-1-induced skeletal myotube hypertrophy by PI(3)K/Akt/mTOR and PI(3)K/Akt/GSK3 pathways. *Nat. Cell Biol.* **3**:1009–1013.
8. Latres, E., et al. 2005. Insulin-like growth factor-1 (IGF-1) inversely regulates atrophy-induced genes via the phosphatidylinositol 3-kinase/Akt/mammalian target of rapamycin (PI3K/Akt/mTOR) pathway. *J. Biol. Chem.* **280**:2737–2744.
9. Cai, D., et al. 2004. IKKbeta/NF-kappaB activation causes severe muscle wasting in mice. *Cell.* **119**:285–298.
10. Sandri, M., et al. 2004. Foxo transcription factors induce the atrophy-related ubiquitin ligase atrogin-1 and cause skeletal muscle atrophy. *Cell.* **117**:399–412.
11. Li, Y.P., Schwartz, R.J., Waddell, I.D., Holloway, B.R., and Reid, M.B. 1998. Skeletal muscle myocytes undergo protein loss and reactive oxygen-mediated NF-kappaB activation in response to tumor necrosis factor alpha. *FASEB J.* **12**:871–880.
12. Greer, E.L., and Brunet, A. 2005. FOXO transcription factors at the interface between longevity and tumor suppression. *Oncogene.* **24**:7410–7425.
13. Lehtinen, M.K., et al. 2006. A conserved MST-FOXO signaling pathway mediates oxidative-stress responses and extends life span. *Cell.* **125**:987–1001.
14. Matsumoto, M., Han, S., Kitamura, T., and Accili, D. 2006. Dual role of transcription factor FoxO1 in controlling hepatic insulin sensitivity and lipid metabolism. *J. Clin. Invest.* **116**:2464–2472. doi:10.1172/JCI27047.
15. Berman, J., and Kenyon, C. 2006. Germ-cell loss extends C. elegans life span through regulation of DAF-16 by kri-1 and lipophilic-hormone signaling. *Cell.* **124**:1055–1068.
16. Lecker, S.H., et al. 2004. Multiple types of skeletal muscle atrophy involve a common program of changes in gene expression. *FASEB J.* **18**:39–51.
17. Kamei, Y., et al. 2004. Skeletal muscle FOXO1 (FKHR) transgenic mice have less skeletal muscle mass, down-regulated Type I (slow twitch/red muscle) fiber genes, and impaired glycemic control. *J. Biol. Chem.* **279**:41114–41123.
18. Skurk, C., et al. 2005. The FOXO3a transcription factor regulates cardiac myocyte size downstream of AKT signaling. *J. Biol. Chem.* **280**:20814–20823.
19. Obsilova, V., et al. 2005. 14-3-3 Protein interacts with nuclear localization sequence of forkhead transcription factor FoxO4. *Biochemistry.* **44**:11608–11617.
20. Hunter, R.B., et al. 2002. Activation of an alternative NF-kappaB pathway in skeletal muscle during disuse atrophy. *FASEB J.* **16**:529–538.
21. Hunter, R.B., and Kandarian, S.C. 2004. Disruption of either the Nfkb1 or the Bcl3 gene inhibits skeletal muscle atrophy. *J. Clin. Invest.* **114**:1504–1511. doi:10.1172/JCI200421696.
22. Acharyya, S., et al. 2005. Dystrophin glycoprotein complex dysfunction: A regulatory link between muscular dystrophy and cancer cachexia. *Cancer Cell.* **8**:421–432.
23. Acharyya, S., et al. 2004. Cancer cachexia is regulated by selective targeting of skeletal muscle gene products. *J. Clin. Invest.* **114**:370–378. doi:10.1172/JCI200420174.
24. Brenman, J.E., Chao, D.S., Xia, H., Aldape, K., and Bredt, D.S. 1995. Nitric oxide synthase complexed with dystrophin and absent from skeletal muscle sarcolemma in Duchenne muscular dystrophy. *Cell.* **82**:743–752.
25. Kameya, S., et al. 1999. Alpha1-syntrophin gene disruption results in the absence of neuronal-type nitric-oxide synthase at the sarcolemma but does not induce muscle degeneration. *J. Biol. Chem.* **274**:2193–2200.
26. Hosaka, Y., et al. 2002. Alpha1-syntrophin-deficient skeletal muscle exhibits hypertrophy and aberrant formation of neuromuscular junctions during regeneration. *J. Cell Biol.* **158**:1097–1107.
27. Lecour, S., et al. 2001. Levels of nitric oxide in the heart after experimental myocardial ischemia. *J. Cardiovasc. Pharmacol.* **37**:55–63.
28. Asanuma, K., et al. 2005. Diffusion of cytotoxic concentrations of nitric oxide generated luminally at the gastro-oesophageal junction of rats. *Gut.* **54**:1072–1077.
29. Nagano, T., and Yoshimura, T. 2002. Bioimaging of Nitric Oxide. *Chem. Rev.* **102**:1235–1270.
30. Kato, N., Sato, S., Yokoyama, H., Kayama, T., and Yoshimura, T. 2005. Sequential changes of nitric oxide levels in the temporal lobes of kainic acid-treated mice following application of nitric oxide synthase inhibitors and phenobarbital. *Epilepsy Res.* **65**:81–91.
31. Moore, P.K., and Bland-Ward, P.A. 1996. 7-nitroindazole: an inhibitor of nitric oxide synthase. *Methods Enzymol.* **268**:393–398.
32. Reynaert, N.L., et al. 2004. Nitric oxide represses inhibitory kappaB kinase through S-nitrosylation. *Proc. Natl. Acad. Sci. U. S. A.* **101**:8945–8950.
33. Hu, M.C., et al. 2004. IkappaB kinase promotes tumorigenesis through inhibition of forkhead FOXO3a. *Cell.* **117**:225–237.
34. Segalat, L., Grisoni, K., Archer, J., Vargas, C., Bertrand, A., and Anderson, J.E. 2005. CAPON expression in skeletal muscle is regulated by position, repair, NOS activity, and dystrophy. *Exp. Cell Res.* **302**:170–179.
35. Shiao, T., et al. 2004. Defects in neuromuscular junction structure in dystrophic muscle are corrected by expression of a NOS transgene in dystrophin-deficient muscles, but not in muscles lacking alpha- and beta1-syntrophins. *Hum. Mol. Genet.* **13**:1873–1884.
36. Kapur, S., Bedard, S., Marcotte, B., Cote, C.H., and Marette, A. 1997. Expression of nitric oxide synthase in skeletal muscle: a novel role for nitric oxide as a modulator of insulin action. *Diabetes.* **46**:1691–1700.
37. Stamler, J.S., and Meissner, G. 2001. Physiology of nitric oxide in skeletal muscle. *Physiol. Rev.* **81**:209–237.
38. Yoshida, M., et al. 1995. Dystrophin-associated protein A0 is a homologue of the Torpedo 87K protein. *FEBS Lett.* **367**:311–314.
39. Yusuf, I., Zhu, X., Kharas, M.G., Chen, J., and Fruman, D.A. 2004. Optimal B-cell proliferation requires phosphoinositide 3-kinase-dependent inactivation of FOXO transcription factors. *Blood.* **104**:784–787.
40. Huang, H., Regan, K.M., Lou, Z., Chen, J., and Tindall, D.J. 2006. CDK2-dependent phosphorylation of FOXO1 as an apoptotic response to DNA damage. *Science.* **314**:294–297.
41. Kandarian, S.C., and Jackman, R.W. 2006. Intracellular signaling during skeletal muscle atrophy. *Muscle Nerve.* **33**:155–165.
42. Mochizuki, Y., et al. 2005. Participation of bone marrow-derived cells in fibrotic changes in denervated skeletal muscle. *Am. J. Pathol.* **166**:1721–1732.

Autologous Transplantation of SM/C-2.6$^+$ Satellite Cells Transduced with Micro-dystrophin *CS1* cDNA by Lentiviral Vector into *mdx* Mice

Madoka Ikemoto[1], So-ichiro Fukada[1], Akiyoshi Uezumi[1], Satoru Masuda[1], Hiroyuki Miyoshi[2], Hiroshi Yamamoto[3], Michiko R Wada[1], Nami Masubuchi[1,4], Yuko Miyagoe-Suzuki[1] and Shin'ichi Takeda[1]

[1]Department of Molecular Therapy, National Institute of Neuroscience, National Center of Neurology and Psychiatry, Kodaira, Tokyo, Japan; [2]BioResource Center, RIKEN Tsukuba Institute, Tsukuba, Ibaraki, Japan; [3]Department of Immunology, Graduate School of Pharmaceutical Sciences, Osaka University, Suita, Osaka, Japan; [4]Laboratory of Molecular Embryology, Department of Bioscience, Kitasato University School of Science, Sagamihara, Kanagawa, Japan

Duchenne muscular dystrophy (DMD) is a lethal muscle disorder caused by mutations in the dystrophin gene. Transplantation of autologous myogenic cells genetically corrected *ex vivo* is a possible treatment for this disorder. In order to test the regenerative efficiency of freshly isolated satellite cells, we purified quiescent satellite cells from limb muscles of 8–12-week-old green fluorescent protein-transgenic (GFP-Tg) mice using SM/C-2.6 (a recently developed monoclonal antibody) and flow cytometry. Freshly isolated satellite cells were shown to participate in muscle regeneration more efficiently than satellite cell-derived myoblasts passaged *in vitro* do, when transplanted into tibialis anterior (TA) muscles of 8–12-week-old cardiotoxin-injected C57BL/6 mice and 5-week-old dystrophin-deficient *mdx* mice, and analyzed at 4 weeks after injection. Importantly, expansion of freshly isolated satellite cells *in vitro* without passaging had no detrimental effects on their regenerative capacity. Therefore we directly isolated satellite cells from 5-week-old *mdx* mice using SM/C-2.6 antibody and cultured them with lentiviral vectors expressing micro-dystrophin *CS1*. The transduced cells were injected into TA muscles of 5-week-old *mdx* mice. At 4 weeks after transplantation, the grafted cells efficiently contributed to regeneration of *mdx* dystrophic muscles and expressed micro-dystrophin at the sarcolemma. These results suggest that there is potential for lentiviral vector-mediated *ex vivo* gene therapy for DMD.

Received 22 February 2007; accepted 28 July 2007; published online 28 August 2007. doi:10.1038/sj.mt.6300295

INTRODUCTION

Duchenne muscular dystrophy (DMD) is an X-linked, lethal disorder of skeletal muscle caused by mutations in the dystrophin gene.[1] Dystrophin is a 427 kd large sub-sarcolemmal protein that forms the dystrophin/glycoprotein complex at the sarcolemma with α- and β-dystroglycans, α-, β-, γ-, and δ-sarcoglycans, and other molecules, and links the cytoskeleton with the basal lamina.[2,3] The lack of dystrophin in the sarcolemma causes instability of the muscle membrane, leading to muscle degeneration and myofiber loss. Although there is no effective treatment for the disease at present, cell therapy could be a promising approach. Satellite cells are quiescent mononucleated cells located external to the muscle membrane but internal to the basal lamina in adult skeletal muscle.[4] On muscle damage, they activate, proliferate, and then exit the cell cycle either to differentiate into mature myofibers or to renew the quiescent satellite cell pool. Because satellite cells have robust regenerative capacity,[5,6] they are expected to be a feasible source for cell therapy in DMD. Indeed, transplantation of myoblasts successfully restored dystrophin expression in dystrophin-deficient muscle under immunosuppression.[7,8] Nevertheless, in the early 90s, transplantation of satellite cell-derived myoblasts failed to improve muscle force in DMD patients.[9–11] The failure has been ascribed to poor survival[12–14] and limited distribution of the transplanted cells after injection.[15] The latter problem could possibly be partly overcome by using high-density injections of myoblasts.[16,17] On the other hand, the mechanisms by which grafted myoblasts are rapidly lost after injection have not been fully addressed.[12–14]

Many studies have employed crude cell preparations containing both satellite cells and non-myogenic cells[18,19] or satellite cell-derived myoblasts extensively amplified *in vitro*.[15,20–22] In a recent study, Montarras *et al.* directly isolated (Pax3)green fluorescent protein (GFP)-expressing satellite cells from the diaphragm of adult *Pax3*$^{GFP/+}$ mice by flow cytometry.[23] These cells constituted a homogeneous population and the majority were quiescent. When grafted into irradiated muscles of immunodeficient *nu/nu* dystrophin-deficient *mdx* mice, the freshly isolated satellite cells efficiently contributed to both fiber repair and the muscle satellite cell compartment,[23] thereby suggesting that fresh satellite cells are a potential source for cell therapy in DMD.

For transplanting autologous cells, which are expected to evade the host immune response to grafted cells, the lentiviral vector is a potential tool for introducing the therapeutic gene

Correspondence: Shin'ichi Takeda, Department of Molecular Therapy, National Institute of Neuroscience, National Center of Neurology and Psychiatry, 4-1-1 Ogawa-higashi, Kodaira, Tokyo 187-8502, Japan. E-mail: takeda@ncnp.go.jp

because it integrates into the host genome in a variety of dividing and non-dividing cells. Because the dystrophin complementary DNA is too large to be incorporated into a lentiviral vector, a truncated but fully functional version of the dystrophin complementary DNA[24–27] has to be used instead of the full-length one. When compared with conventional transfection of myogenic cells with large dystrophin-coding plasmids[28] or nucleofection in combination with ϕC31 integrase,[29] transfection by lentiviral vectors led to much more efficient expression of mini- or micro-dystrophin in *mdx* mice,[30] in non-human primate cells, and in human myogenic cells.[31] Lentiviral vectors were also used for introducing the therapeutic genes into other types of stem cells. Bachrach *et al.* reported expression of human micro-dystrophin in *mdx*^{5cv} muscles after systemic delivery of autologous side population cells modified with lentiviral vectors expressing micro-dystrophin.[32] Sampaolesi *et al.* reported intra-arterial delivery of autologous mesoangioblasts corrected by lentiviral vectors expressing α-sarcoglycan (α-SG), resulting in many α-SG-positive fibers, and morphological and functional recovery in downstream muscles of α-SG-null dystrophic mice.[33] A more recent study reported the autologous transplantation into skeletal muscle, of monkey muscle precursor cells transduced with micro-dystrophin by lentiviral vectors.[31] However, whether *ex vivo* gene therapy using lentiviral vectors expressing micro-dystrophin is indeed beneficial in large animal models such as dystrophic dogs, is still subject to controversy.[34]

Previously, Fukada *et al.* established a method of direct purification of quiescent satellite cells from adult mouse skeletal muscles, using fluorescence activated cell sorting (FACS) and a novel monoclonal antibody named SM/C-2.6.[35] The method is simple, and is expected to be applicable to the isolation of satellite cells from dystrophic (autologous) muscles for cell therapy.

In this study, we first directly isolated satellite cells from *mdx* mice using the SM/C-2.6 antibody and FACS. We showed that *mdx*-SM/C-2.6$^+$ cells transduced with lentiviral vectors expressing micro-dystrophin efficiently contributed to regeneration of *mdx* muscles and expressed micro-dystrophin at the sarcolemma when grafted. Our results indicate that the autologous satellite cell isolated by the SM/C-2.6 antibody and genetically corrected by a lentiviral vector is a feasible tool for cell therapy of DMD or of localized forms of muscular dystrophy.

RESULTS

Passaged SM/C-2.6$^+$ satellite cells show reduced regenerative capacity

We isolated satellite cells from the limb muscles of 8–12-week-old C57BL/6 mice using FACS and a novel monoclonal antibody, SM/C-2.6.[35] A previous study has shown that satellite cells are highly enriched in the SM/C-2.6$^+$ fraction.[35] Immediately after isolation by FACS, SM/C-2.6$^+$ cells expressed Pax7, but not MyoD, myogenin, or Ki67 (**Table 1**). After 4 days of culture, more than 95% of the cells expressed MyoD and Ki67 (data not shown). Pax7 marks quiescent, activated satellite cells and their progeny, myoblasts,[36] whereas MyoD marks activated satellite cells and myoblasts.[37,38] Ki67 is a marker of proliferating cells. It follows, therefore, that SM/C-2.6$^+$ cells are highly purified satellite cells in the G_0 phase immediately after isolation from muscle tissues.

Table 1 Expression of myogenic and proliferative markers of freshly isolated SM/C-2.6$^+$ cells from limb muscles of C57BL/6 or *mdx* mice

Marker	B6-SM/C-2.6$^+$ cells (%)	*mdx*-SM/C-2.6$^+$ cells (%)
Pax7	95 ± 1.4	94 ± 2.1
MyoD	0 ± 0	19 ± 2.8
Myogenin	0 ± 0	7 ± 1.3
Ki67	0.6 ± 1.0	34 ± 1.8

The expression level of each marker is shown as the percentage of positive cells in total cells stained with 4',6-diamidino-2-phenylindole in three randomly selected fields. Data are represented as mean values ± SD.

To investigate the regenerative efficiency of SM/C-2.6$^+$ satellite cells when grafted into mouse skeletal muscles, three kinds of cells were prepared from limb muscles of 8–12-week-old GFP-Tg mice: (i) quiescent SM/C-2.6$^+$ cells freshly isolated by FACS (**Figure 1a**), (ii) expanded SM/C-2.6$^+$ cells *in vitro* with or without passaging (**Figure 1a**), and (iii) cultured primary myoblasts isolated by a conventional pre-plating method.[39] These cells were injected at 2×10^4 cells per muscle into the tibialis anterior (TA) muscle of 8–12-week-old C57BL/6 and 5-week-old dystrophin-deficient *mdx* mice. Twenty four hours before cell transplantation the recipient C57BL/6 muscles were injected with cardiotoxin (CTX) so as to induce regeneration. Four weeks after the injection, we investigated the contribution of each cell population to muscle regeneration by immunodetection of GFP-positive fibers. Freshly isolated SM/C-2.6$^+$ cells (**Figure 1b**) produced many more GFP-positive fibers than those produced by the same number of cultured SM/C-2.6$^+$ cells passaged once *in vitro* (**Figure 1c**, passage 1). We next examined the effects of expansion, without passaging and with repeated passaging, on the regenerative capacity of the cells. The number of GFP-positive myofibers derived from GFP-Tg SM/C-2.6$^+$ cells dropped considerably after first passage *in vitro* and then gradually decreased with subsequent passages in both CTX-injected C57BL/6 mice (**Figure 1d**) and in *mdx* mice (**Figure 1e**). Primary myoblasts prepared by the pre-plating method[39] also showed low regenerative capacity (**Figure 1d**). Surprisingly, the regenerative efficiency of cells expanded *in vitro* without passaging was comparable to that of freshly isolated cells (**Figure 1d** and **e**). These results suggested to us that it is possible to genetically correct dystrophin-deficient satellite cells *ex vivo* before transplantation without causing a reduction in their regenerative capacity.

In order to know why fresh or "expansion" cells gave rise to more myofibers when compared with cells passaged *in vitro*, we compared the colony formation ability of fresh satellite cells with that of passaged myoblasts (passage 1). The results showed that fresh satellite cells formed larger colonies than passage 1 cells, when plated at a density of 1 cell/well on 96-well plates, although the rate of colony formation was not significantly different between these two cells (fresh, 26% versus passage 1, 23%) (**Supplementary Figure S1**). In contrast, there was no difference in fusion index between fresh satellite cells and passaged myoblasts (data not shown). Collectively, a reduction in the proliferative ability of passaged myoblasts *in vitro* might partly explain their lower regenerative capacity *in vivo*.

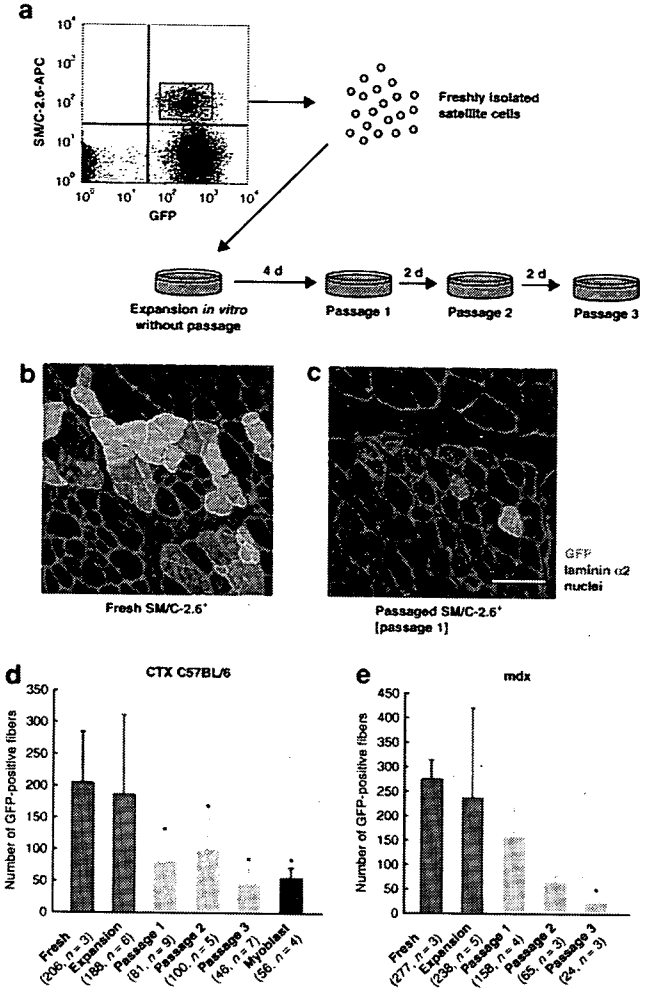

Figure 1 The regenerative capacity of SM/C-2.6$^+$ satellite cells isolated from adult mouse skeletal muscles by fluorescence activated cell sorting (FACS). **(a)** Flow cytometry of mononucleated cells derived from limb muscles of green fluorescent protein-transgenic (GFP-Tg) mice after staining with SM/C-2.6 antibody and culture conditions of sorted cells. SM/C-2.6$^+$ GFP$^+$ cells (red square) were sorted as the satellite cell fraction. These cells were cultured in proliferation medium for 4 days (expansion *in vitro* without passage) and then passaged up to three times at 2-day intervals. **(b)** Freshly isolated and **(c)** passaged SM/C-2.6$^+$ cells (passage 1) from GFP-Tg mice were injected into C57BL/6 tibialis anterior (TA) muscles. The muscles were treated with cardiotoxin (CTX) 24 hours before cell transplantation and then injected with 2 × 10^4 cells per TA muscle. Four weeks after the injection, cross-sections were stained with anti-GFP (green) and laminin α2 (red) antibodies. Nuclei were stained with TOTO3 (blue). Bar: 80 μm. **(d, e)** Comparison of muscle regenerative efficiencies of three kinds of cells prepared from GFP-Tg mice: (i) quiescent SM/C-2.6$^+$ cells freshly isolated by FACS (red bars), (ii) expanded SM/C-2.6$^+$ cells *in vitro* without passaging (orange bars) or passaged SM/C-2.6$^+$ cells (yellow bars with passage numbers), and (iii) primary myoblasts isolated by the preplating method (blue bar in **d**). The same numbers of cells (2 × 10^4 cells) were grafted into TA muscles of CTX-treated C57BL/6 (d) and *mdx* mice **(e)**. The number of GFP-positive fibers per cross-section was counted after staining with anti-GFP antibody. Error bars represent SD. $^*P < 0.05$ compared with freshly isolated SM/C-2.6$^+$ cells.

SM/C-2.6$^+$ satellite cells transduced with lentiviral vectors efficiently contribute to muscle regeneration

Successful gene and cell therapy for DMD requires sustained expression of the therapeutic gene in striated muscle. The

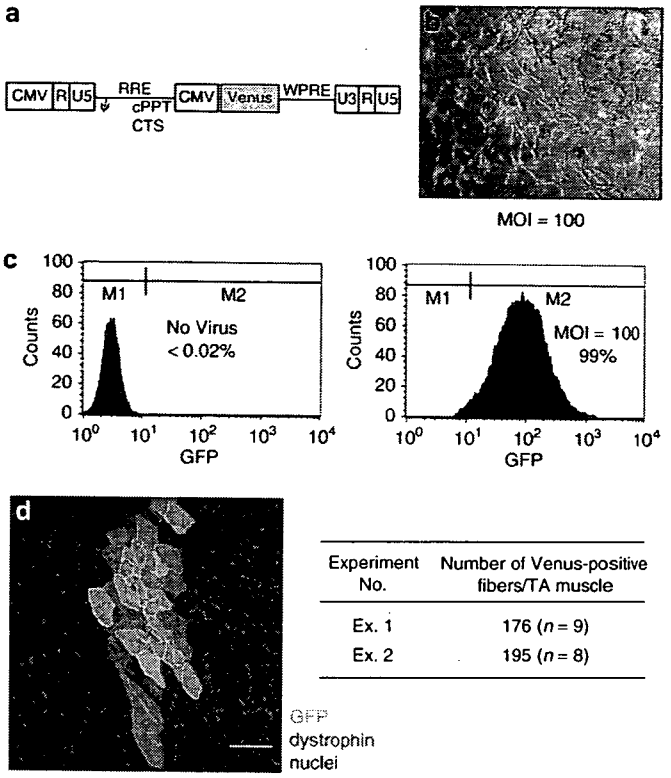

Experiment No.	Number of Venus-positive fibers/TA muscle
Ex. 1	176 (n = 9)
Ex. 2	195 (n = 8)

Figure 2 Lentiviral vector-mediated gene transfer into SM/C-2.6$^+$ satellite cells and transplantation of transduced cells into *mdx* mouse muscles. **(a)** Structure of the lentiviral vector expressing Venus under the control of a cytomegalovirus (CMV) promoter. **(b)** Fluorescence of Venus-expressing satellite cell-derived myoblasts. Freshly isolated SM/C-2.6$^+$ cells from C57BL/10 limb muscles were transduced with lentiviral vectors expressing Venus at a multiplicity of infection (MOI) of 100 for 16 hours, and cultured in proliferation medium for 3 days. **(c)** Flow cytometric analysis of non-transduced (left panel) and transduced (right panel) SM/C-2.6$^+$ cells 3 days after the transduction. M2 denotes the area of Venus-expressing cells. At a MOI of 100, 99% of the cells expressed Venus. **(d)** Venus- and dystrophin-positive fibers formed by SM/C-2.6$^+$ cells transduced with lentiviral vectors *in vitro*. Transduced cells (2 × 10^4) were injected into tibialis anterior (TA) muscles of *mdx* mice. Four weeks after the injection, cross-sections were stained with anti-GFP (green) and dystrophin (red) antibodies. Nuclei were stained with TOTO3 (blue). The number of Venus-positive fibers per cross-section was counted. Bar: 80 μm. cPPT, central polypurine tract; CTS, central termination sequence; GFP, green fluorescent protein; RRE, rev responsive element; WPRE, woodchuck hepatitis virus post-transcriptional regulatory element.

lentiviral vector can carry a relatively large transgene and integrate it into the genome of non-dividing cells such as quiescent satellite cells. We therefore attempted lentiviral vector–mediated gene transfer into satellite cells. For this purpose, we used a human immunodeficiency virus-1–based lentiviral vector pseudotyped with vesicular stomatitis virus-G glycoprotein.[40] To start with, we used a vector that expresses Venus, a variant of yellow fluorescent protein[41] under the control of a cytomegalovirus (CMV) promoter (**Figure 2a**). Freshly isolated satellite cells from limb muscles of 8–12-week-old C57BL/10 mice, which are syngenic to *mdx*, were transduced with the lentiviral vectors at a multiplicity of infection (MOI) of 100 for 16 hours. After removal of free viral vectors and *in vitro* expansion of the cells for 3 days, numerous Venus-positive cells were detected (**Figure 2b**). Flow

cytometric analyses revealed that 99% of the SM/C-2.6$^+$ satellite cell–derived myoblasts expressed Venus when transduced at a MOI of 100 (**Figure 2c**, right panel). These transduced cells were injected into TA muscles of 5-week-old *mdx* mice at 2×10^4 per muscle. Four weeks after the injection, the muscle regeneration capacity of cells transduced with lentiviral vectors was investigated by immunodetection of Venus- or dystrophin-positive fibers. As in the case of the non-transduced cells (**Figure 1d** and **e**), grafting of transduced cells too led to many Venus- and dystrophin-positive fibers (**Figure 2d**). This serves to show that SM/C-2.6$^+$ satellite cell-derived myoblasts transduced with lentiviral vectors contribute efficiently to muscle regeneration.

Direct isolation of SM/C-2.6$^+$ satellite cells from dystrophic muscles of *mdx* mice

In order to test whether autologous myogenic precursor cells genetically corrected to express a dystrophin gene represent a possible tool in DMD therapy, we next attempted to directly isolate SM/C-2.6$^+$ cells from limb muscles of 5-week-old *mdx* mice. Numerous inflammatory and fibroblastic cells reflecting the active cycles of the degeneration–regeneration process are found in dystrophic muscles. SM/C-2.6 antibody reacts with activated fibroblastic cells (Fukada *et al.*, unpublished data). Because satellite cells are negative for both Sca-1 and CD31,[35] we stained *mdx* muscle-derived mononuclear cells with a cocktail of CD45, CD31, Sca-1, and SM/C-2.6 antibodies and collected SM/C-2.6$^+$ CD45$^-$ CD31$^-$ Sca-1$^-$ cells as the satellite cell fraction (**Figure 3a**). When these cells were cultured in proliferation medium for 4 days, more than 95% of them expressed MyoD (**Figure 3b**). These results indicate that, using the SM/C-2.6 antibody, a pure population of satellite cells can be isolated, not only from wild-type muscle but also from dystrophic muscle of *mdx* mice. Immediately after isolation, the majority of satellite cells from C57BL/6 mice were negative for MyoD, myogenin, and Ki67. On the other hand, 19% of *mdx*-satellite cells were positive for MyoD and 34% of the cells were positive for Ki67 (**Table 1**). There was no difference between *mdx*- and B6-SM/C-2.6$^+$ cells with respect to expression of Pax7 (**Table 1**). This proves that a considerable fraction of satellite cells are in an activated, proliferative state in skeletal muscles of *mdx* mice.

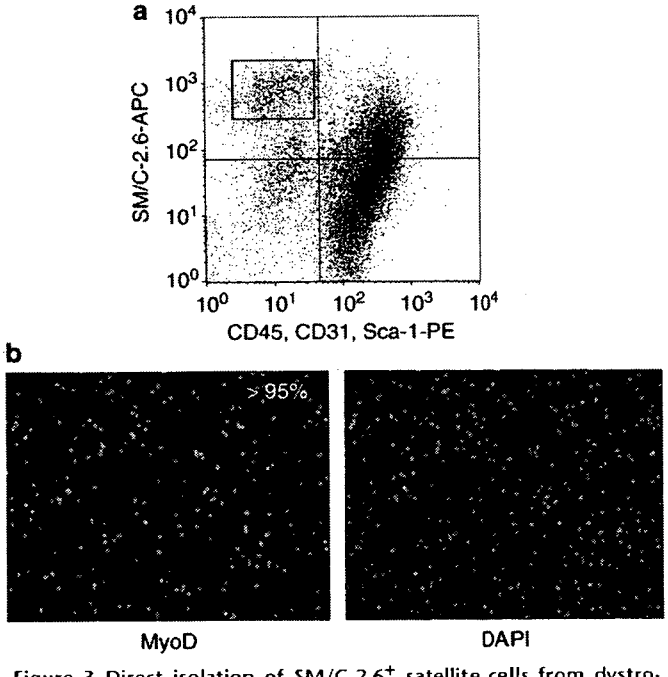

Figure 3 Direct isolation of SM/C-2.6$^+$ satellite cells from dystrophic muscles of *mdx* mice. (**a**) Flow cytometry of mononucleated cells derived from *mdx* mice, and stained with a cocktail of CD45, CD31, Sca-1, and SM/C-2.6 antibodies. SM/C-2.6$^+$ CD45$^-$ CD31$^-$ Sca-1$^-$ cells (red square) were sorted as the satellite cell fraction. (**b**) Sorted *mdx*-satellite cells were cultured in proliferation medium for 4 days and stained with anti-MyoD antibody (green) and 4′,6-diamidino-2-phenylindole (DAPI) (nuclei, blue). More than 95% of them expressed MyoD.

Successful micro-dystrophin gene transfer into *mdx*-SM/C-2.6$^+$ satellite cells

The full-length dystrophin complementary DNA, at 14 kilobase (kb), is too large to be incorporated into a lentiviral vector. In previous studies, we constructed a rod-truncated micro-dystrophin *CS1* and demonstrated that it effectively rescued

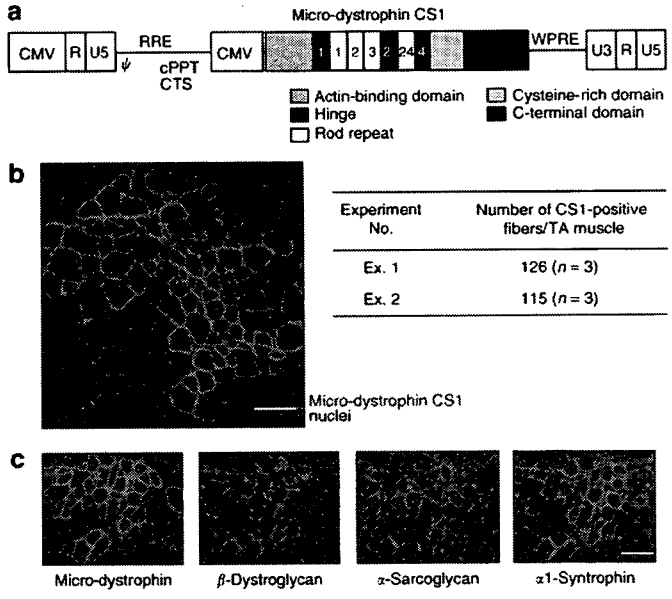

Figure 4 Lentiviral vector-mediated micro-dystrophin *CS1* gene transfer into *mdx*-SM/C-2.6$^+$ cells and transplantation of transduced cells into *mdx* muscles. (**a**) Structure of the lentiviral vector expressing micro-dystrophin *CS1*. *CS1* complementary DNA was inserted downstream of the cytomegalovirus (CMV) promoter. *CS1* has the N-terminal domain, a shortened version of the central rod domain with four rod repeats and three hinges, the cysteine-rich domain, and the C-terminal domain. The numbers of rod repeats and hinges are also shown. (**b**) Freshly isolated SM/C-2.6$^+$ cells from *mdx* dystrophic muscles were transduced with lentiviral vectors expressing micro-dystrophin *CS1* at a multiplicity of infection of 200 for 16 hours and cultured in proliferation medium for 2 days. Transduced cells (2×10^4) were injected into *mdx* tibialis anterior (TA) muscles. Four weeks after the injection, cross-sections were stained with anti-dystrophin antibody (red) and TOTO3 (nuclei, blue). The number of micro-dystrophin *CS1*-positive fibers per cross-section was counted. Bar: 80 μm. (**c**) Restoration of dystrophin-associated proteins at the sarcolemma of micro-dystrophin-positive fibers. Serial cross-sections were stained with anti-dystrophin, β-dystroglycan, α-sarcoglycan, and α1-syntrophin antibodies (red), and TOTO3 (nuclei, blue). Bar: 80 μm. cPPT, central polypurine tract; CTS, central termination sequence; RRE, rev responsive element; WPRE, woodchuck hepatitis virus post-transcriptional regulatory element.

the dystrophic phenotypes of *mdx* mice when introduced as a transgene[24] or by adeno-associated viral vectors.[25] We therefore inserted a 4.9 kb micro-dystrophin *CS1* into the lentiviral vector as a therapeutic gene. Freshly isolated *mdx*-SM/C-2.6$^+$ cells were transduced with lentiviral vectors expressing micro-dystrophin *CS1* under the control of a CMV promoter (**Figure 4a**) at a MOI of 200 for 16 hours. In this condition, 97% of the cells expressed micro-dystrophin *CS1* (data not shown). These transduced cells were injected into TA muscles of 5-week-old *mdx* mice at 2×10^4 cells per muscle. Four weeks after the injection, the muscle regeneration capacity of the cells was investigated by immunodetection of micro-dystrophin-positive fibers. Many myofibers expressed micro-dystrophin *CS1* on the sarcolemma at an average of 120 fibers per muscle (**Figure 4b**). Further, we examined the restoration of the dystrophin-associated protein complex in micro-dystrophin-positive fibers by immunodetection of α-SG, β-dystroglycan, and α1-syntrophin. As shown in **Figure 4c**, all these proteins were expressed at the sarcolemma of micro-dystrophin *CS1*-positive myofibers, thereby suggesting the recovery of dystrophin-associated protein complex by the introduction of micro-dystrophin. These results indicate that *mdx*-SM/C-2.6$^+$ cells transduced with lentiviral vectors expressing micro-dystrophin *CS1* efficiently contribute to regeneration of dystrophic muscles of *mdx* mice and restore the expression of the dystrophin/dystrophin-associated protein complex. It therefore follows that transplantation of autologous myogenic precursor cells prepared using the SM/C-2.6 antibody and genetically corrected by a lentiviral vector, is a possible approach for cell therapy in DMD or in localized forms of muscular dystrophy.

DISCUSSION

In vitro *passaging reduced the regenerative capacity of satellite cells*: In the present study, we directly isolated satellite cells from skeletal muscles of wild-type and *mdx* mice using SM/C-2.6, a novel monoclonal antibody,[35] and flow cytometry. Almost all satellite cells prepared from normal muscle are negative for MyoD, myogenin, and Ki67 immediately after isolation, thereby indicating that they are in a quiescent state. In contrast, approximately 20% of *mdx*-satellite cells are positive for MyoD and 35% are positive for Ki67 (**Table 1**). This result indicates that a fraction of *mdx*-satellite cells are already in an activated state.

Transplantation experiments showed that freshly isolated SM/C-2.6$^+$ satellite cells possess a higher capacity for muscle reconstitution when compared with SM/C-2.6$^+$ myoblasts passaged *in vitro* prior to transplantation. This result indicates that passaging and subsequent proliferation of satellite cells in culture reduce their intrinsic capacity for muscle reconstitution. In order to clarify the mechanisms of low myogenicity of passaged cells, we performed a colony-forming assay of freshly isolated satellite cells and passaged satellite cell-derived myoblasts (passage 1). When the cells were seeded at a density of 1 cell/well on 96-well plates, fresh satellite cells formed larger colonies than "passage 1" myoblasts (**Supplementary Figure S1**). In contrast, there was no difference in fusion index between these two cell populations (data not shown). Collectively, reduced efficiency of muscle fiber regeneration by passaged myoblasts can be partly explained by gradual loss of proliferative ability during passaging.

Importantly, we also found that satellite cells that were expanded *in vitro* without passaging showed regenerative capacity comparable to freshly isolated satellite cells. We therefore hypothesized that it might be possible to introduce therapeutic genes into satellite cells *in vitro* by a lentiviral vector before transplantation without causing any reduction in their regenerative capacity.

Comparison of regenerative capacity of SM/C-2.6$^+$ satellite cells with other reports: Previously, Montarras *et al.* directly isolated (Pax3) GFP-expressing satellite cells, which constitute a homogeneous population of small, non-granular, CD34$^+$ CD45$^-$ Sca-1$^-$ cells, from diaphragms of adult *Pax3*$^{GFP/+}$ mice by flow cytometry, and examined their regenerative capacity.[23] The researchers concluded that *in vitro* expansion of freshly isolated satellite cells for a few days prior to transplantation is a disadvantageous approach, because such satellite cell-derived myoblasts displayed considerably lower muscle regenerative efficiency than fresh satellite cells. In contrast, we observed no reduction in regenerative capacity as a result of *in vitro* expansion of freshly isolated satellite cells without passaging, although their capacity was remarkably reduced after passaging (**Figure 1d** and **e**). The discrepancy between the results of Montarras *et al.* and our results may be due to differences in the culture conditions employed. One possible explanation could be that our culture medium contained basic fibroblast growth factor. It has been reported that addition of basic fibroblast growth factor to culture medium improves transplantation efficiency.[42,43] The modification of culture conditions may enable maintenance of the intrinsic muscle regenerative capacity of satellite cells.

Previous muscle transplantation experiments utilized the progeny of satellite cells enzymatically dissociated from myofibers and extensively cultured to increase their numbers.[15,20–22] When 5×10^5 to 1×10^6 myoblasts taken from normal mice and prepared by the pre-plating method were transplanted into non-irradiated muscles of *mdx* mice, it resulted in fewer than 100 dystrophin-positive myofibers per muscle.[21] On the other hand, when 5×10^5 cells were injected into muscles of immunodeficient *mdx nu/nu* mice that had been pre-irradiated to ablate endogenous satellite cell function, they formed an average of 328 dystrophin-positive fibers.[18] Furthermore, grafting of 2×10^4 satellite cells freshly isolated from *Pax3*$^{GFP/+}$ mice into pre-irradiated TA muscles of *mdx nu/nu* mice led to dystrophin expression in an average of 587 fibers.[23] In our experiment, the same number (2×10^4) of satellite cells freshly isolated from adult normal mice gave rise to an average of only 277 myofibers in non-irradiated *mdx* muscles (**Figure 1d** and **e**). This shows that grafted muscle precursor cells form a far greater number of dystrophin-positive fibers in irradiated muscle than in non-irradiated muscle. The use of immunosuppressants such as FK506 also greatly improves the efficiency of transplantation.[7] In the present study, we injected myogenic cells into non-irradiated TA muscles of immunocompetent mice without any immunosuppressant. Therefore, in our experimental

conditions, the intrinsic function of SM/C-2.6$^+$ satellite cells may be underestimated.

The use of the Lentiviral vector is feasible for ex vivo *gene transfer*: In this study we showed that, at a MOI of 200, lentiviral vectors can introduce the rod-truncated micro-dystrophin gene *CS1* into more than 97% of *mdx*-satellite cells without detrimental effects on cell viability and regenerative capacity. But at a MOI of 300 we observed cell toxicity, whereas at a MOI of 100, the transduction efficiency was below 80% (data not shown). When we injected the transduced autologous myoblasts into *mdx* muscle, the cells contributed to regeneration of myofibers and expressed micro-dystrophin and dystrophin-associated proteins at the sarcolemma. Our results therefore suggest that *ex vivo* gene transfer into autologous myogenic cells by a lentiviral vector is feasible. On the other hand, direct intramuscular injection of vesicular stomatitis virus-G glycoprotein–pseudotyped lentiviral vectors led to relatively low expression of the transgene in mouse skeletal muscles.[30,44] Because the lentiviral vector genome is inserted into the host genome, the transduction of cells other than the target cell could introduce the risk of mutagenesis. Further, *in vivo* administration could induce undesirable immune responses to exogenous viral proteins. In effect, direct *in vivo* administration of lentiviral vectors poses a safety problem for clinical application. In contrast, *ex vivo* gene transfer has the merit of minimizing the risks of introducing free lentiviral vectors into the host. Transduced cells can efficiently proliferate and differentiate *invitro* (data not shown).

Limitations of ex vivo *gene therapy in DMD, using satellite cells*: One of the demerits of our procedure, as compared to *in vivo* gene transfer, is that only a part of the genetically modified myogenic precursor cells contributes to regeneration of the host muscle, given the poor survival rate of these cells. In fact, by using real-time polymerase chain reaction on transcripts from the transgenic enhanced GFP gene, we found that more than 90% of the injected cells were lost within the first 24 hours after injection (data not shown). In addition, migration of the surviving cells is limited in the host muscle after injection. Furthermore, because *in vitro* passaging greatly reduces their myogenicity, it is difficult to obtain a sufficient number of satellite cells or their progeny from a small muscle biopsy of a DMD patient. Therefore current myoblast transfer might be more realistic for localized forms of muscular dystrophy, such as oculo-pharyngeal muscular dystrophy or facio-scapulo-humeral muscular dystrophy.[45] Surprisingly, however, Collins *et al.* transplanted a single intact myofiber into irradiation-ablated muscles and demonstrated that as few as seven satellite cells associated with one transplanted myofiber can generate over 100 new myofibers containing thousands of myonuclei.[5] Their observations suggest that proper isolation and handling of satellite cells might greatly improve their myogenic potential.

In this study we have demonstrated transplantation of autologous satellite cells genetically corrected by a lentiviral vector *ex vivo* into *mdx* muscle. For treating DMD patients, however, it is necessary to find the optimum *in vitro* culture condition that will enable human muscle precursor cells to maintain their intrinsic myogenic potential. It would also be useful to identify the factors that support survival and/or proliferation of transplanted cells in the host muscle.

MATERIALS AND METHODS

Animals. All procedures used on the experimental animals were approved by the Experimental Animal Care and Use Committee at the National Institute of Neuroscience. Eight-to-twelve-week-old C57BL/6 mice were purchased from Nihon CLEA (Tokyo, Japan). C57BL/6-GFP Tg mice were kindly provided by Dr. Okabe (Osaka University, Japan). C57BL/10 mice and C57BL/10-*mdx* mice were maintained in our animal facility and propagated by allowing mating.

In order to induce muscle regeneration, 50 µl of CTX (10 µmol/l in saline; Wako Pure Chemical Industries, Tokyo, Japan) was injected into the TA muscle 24 hours before cell transplantation.

Cell preparation and FACS analysis. Freshly isolated muscle-derived cells were prepared from 8–12-week-old GFP-Tg mice, C57BL/6 mice, C57BL/10 mice, or 5-week-old *mdx* mice as previously described.[35] Hind-limb and fore-limb muscles were isolated and digested with 0.2% type II collagenase (Worthington Biochemical, Lakewood, NJ) for 90 minutes at 37 °C. The muscle slurries were filtered through 100 µm nitrex mesh (BD Biosciences, Franklin Lakes, NJ) and subsequently through 40 µm nitrex mesh (BD Biosciences, Franklin Lakes, NJ). Erythrocytes were eliminated by treatment with 0.8% NH_4Cl in Tris-buffer. Mononucleated cells were stained with biotinylated SM/C-2.6 monoclonal antibody,[35] and labeled by allophycocyanin-conjugated streptavidin (BD PharMingen, San Diego, CA). Mononucleated cells derived from *mdx* muscles were stained with antibodies to additional surface markers, phycoerythrin-conjugated anti-CD45 antibody (clone 30-F11; BD PharMingen, San Diego, CA), phycoerythrin-conjugated anti-CD31 antibody (clone 390; BD PharMingen, San Diego, CA), and phycoerythrin-conjugated anti-Sca-1 antibody (clone D7; BD PharMingen, San Diego, CA). After being washed, stained cells were re-suspended in phosphate-buffered saline (PBS) containing 2% fetal bovine serum (Trace Biosciences, New South Wales, Australia) and 2 µg/ml propidium iodide (BD PharMingen, San Diego, CA). Cell sorting was performed on a FACS VantageSE flow cytometer (BD Biosciences, Franklin Lakes, NJ). Debris and dead cells were excluded by forward scatter, side scatter, and propidium iodide gating. We used only propidium iodide-negative fractions for further experiments. We usually obtained approximately 1.5×10^5 sorted cells from 1 g of muscle of 8–12-week-old female C57BL/6 mice.

Cell culture and intramuscular transplantation. Freshly isolated SM/C-2.6$^+$ cells from GFP-Tg mice were seeded at a density of 1×10^5 cells per 35-mm dish coated with Matrigel (BD Biosciences, Franklin Lakes, NJ) in a growth medium, Dulbecco's modified Eagle's medium (Invitrogen, Carlsbad, CA) containing 20% fetal bovine serum and 2.5 ng/ml basic fibroblast growth factor (Invitrogen, Carlsbad, CA), and expanded for 4 days. Further, these cells were passaged up to three times at 2-day intervals. Primary myoblasts isolated by the pre-plating method[39] from GFP-Tg mice were also cultured in growth medium. Freshly sorted cells, expanded and passaged cells, or cultured primary myoblasts were injected into TA muscles of 8–12-week-old CTX-treated C57BL/6 mice or 5-week-old *mdx* mice that show active cycles of the degeneration–regeneration process. The number of injected cells was 2×10^4 per TA muscle. Four weeks later, the injected muscles were isolated and fixed in 4% paraformaldehyde for 30 minutes, immersed sequentially in 10% sucrose/PBS and 20% sucrose/PBS, and frozen in isopentane cooled with liquid nitrogen.

Immunohistochemistry. Frozen muscle tissues were sectioned (6 µm) using a cryostat. The sections were blocked with 5% goat serum (Cedarlane, Hornby, Canada) in PBS and then reacted with anti-GFP antibody (1:100; Chemicon International, Temecula, CA) and/or anti-laminin $\alpha 2$ antibody (1:100; Alexis, San Diego, CA), or anti-$\alpha 1$-syntrophin antibody

(1:500)[46] at 4 °C overnight. Dystrophin (1:20; NCL-DYSB or DYS2; Novocastra, Newcastle, UK), α-SG (1:50; NCL-α-SARC; Novocastra, Newcastle, UK), and β-dystroglycan (1:50; NCL-β-DG; Novocastra, Newcastle, UK) were detected using monoclonal antibodies after blocking with a MOM kit (Vector Laboratories, Burlingame, CA). The sections were incubated with appropriate combinations of Alexa 488-, Alexa 568-, and Alexa 594-labeled secondary antibodies (Molecular Probes, Eugene, OR) for 30 minutes. The nuclei were counterstained with TOTO-3 (1:5,000; Molecular Probes, Eugene, OR). The stained sections were observed under the confocal laser scanning microscope system TCSSP (Leica, Heidelberg, Germany).

Immunocytochemistry. Cells sorted using FACS were collected by Cytospin3 (Thermo Fisher Scientific, Waltham, MA). After being fixed with 4% paraformaldehyde for 10 minutes, the cells were blocked with 5% goat serum in PBS and then reacted with anti-Pax7 antibody (1:2; Developmental Studies Hybridoma Bank, Iowa, IA), anti-MyoD antibody (1:200; Dako, Glostrup, Denmark), anti-myogenin antibody (1:200; Developmental Studies Hybridoma Bank, Iowa, IA), and anti-Ki67 antibody (1:2, Ylem, Rome, Italy) at 4 °C overnight. Primary antibodies were detected by Alexa 488- or Alexa 568-labeled secondary antibodies (Molecular Probes, Eugene, OR) for 30 minutes. Stained cells were mounted in Vectashield with 4′,6-diamidino-2-phenylindole (Vector Laboratories, Burlingame, CA) and observed with fluorescence microscopy IX70 (Olympus, Tokyo, Japan).

Generation of lentiviral vectors and* in vitro *transduction. The third-generation self-inactivated human immunodeficiency virus-1-based lentiviral vector, pCSII-CMV-IRES2-Venus, has been described previously.[47] The vector contains a CMV promoter; an internal ribosomal entry site (IRES) followed by *Venus*, which is a variant of yellow fluorescent protein[41]; and a woodchuck hepatitis virus post-transcriptional regulatory element. A rod-truncated micro-dystrophin *CS1* complementary DNA (four rod repeats, 4.9 kb) was excised from pCAG-*CS1*[24] and cloned into pCSII-CMV-IRES2-Venus, generating pCSII-CMV-*CS1*-IRES2-Venus. The lentiviral vectors expressing Venus only, or micro-dystrophin *CS1* followed by Venus, were generated by transient cotransfection of the pCSII-CMV-IRES2-Venus or pCSII-CMV-*CS1*-IRES2-Venus, respectively, with the packaging construct (pCAG-HIVgp), vesicular stomatitis virus-G protein, and Rev-expressing construct (pCMV-VSV-G-RSV-Rev) into 293T cells, using the calcium phosphate transfection method.[47–49] Two days after transfection, the vector-containing supernatant was collected, filtered through a 0.45-μm-pore-size filter (Thermo Fisher Scientific, Waltham, MA), and concentrated by centrifugation twice at 50,000*g* for 2 hours at 20 °C. The virus pellet was re-suspended in Hank's Balanced Salt Solution (Invitrogen, Carlsbad, CA) and stored at −80°C until use. The titer of the concentrated virus was 5×10^8 to 1×10^9 infectious units/ml when assayed on 293T cells, and infectivity was determined by Venus expression as analyzed on a FACS VantageSE (BD Biosciences, Franklin Lakes, NJ).

Sixty thousand freshly isolated SM/C-2.6$^+$ cells in 300 μl growth medium were seeded in each well of 24-well plates and cultured for 16 hours with viral vectors expressing Venus or micro-dystrophin *CS1* at MOI of 100 or 200, respectively. After removal of free viral vectors by changing the medium, the transduced cells were cultured for 2 or 3 days and trypsinized. A cell suspension containing 2×10^4 cells in 20 μl of PBS was injected into the TA muscles of *mdx* mice. The infection efficiency of the injected cells was evaluated using a FACS VantageSE (BD Biosciences, Franklin Lakes, NJ).

ACKNOWLEDGMENTS

This work was supported by Research on Nervous and Mental Disorders (16B-2), and Health Science Research Grants for Research on the Human Genome and Gene Therapy (H16-genome-003), for Research on Brain Science (H15-kokoro-021, H18-kokoro-019) from the Japanese Ministry of Health, Labor and Welfare, Grants-in-Aids for Scientific Research (14657158, 15390281, 16590333, and 18590392) from the Japanese Ministry of Education, Culture, Sports, Science and Technology, and the "Ground-based Research Program for Space Utilization" promoted by the Japan Space Forum.

SUPPLEMENTARY MATERIAL

Figure S1. Freshly isolated satellite cells give rise to larger colonies than passaged myoblasts *in vitro*.

REFERENCES

1. Emery, AE (1993). Duchenne muscular dystrophy—Meryon's disease. *Neuromuscul Disord* **3**: 263–266.
2. Ervasti, JM and Campbell, KP (1993). A role for the dystrophin-glycoprotein complex as a transmembrane linker between laminin and actin. *J Cell Biol* **122**: 809–823.
3. Suzuki, A, Yoshida, M, Hayashi, K, Mizuno, Y, Hagiwara, Y and Ozawa, E (1994). Molecular organization at the glycoprotein-complex-binding site of dystrophin. Three dystrophin-associated proteins bind directly to the carboxy-terminal portion of dystrophin. *Eur J Biochem* **220**: 283–292.
4. Charge, SB and Rudnicki, MA (2004). Cellular and molecular regulation of muscle regeneration. *Physiol Rev* **84**: 209–238.
5. Collins, CA, Olsen, I, Zammit, PS, Heslop, L, Petrie, A, Partridge, TA *et al.* (2005). Stem cell function, self-renewal, and behavioral heterogeneity of cells from the adult muscle satellite cell niche. *Cell* **122**: 289–301.
6. Schultz, E (1996). Satellite cell proliferative compartments in growing skeletal muscles. *Dev Biol* **175**: 84–94.
7. Kinoshita, I, Vilquin, JT, Guerette, B, Asselin, I, Roy, R and Tremblay, JP (1994). Very efficient myoblast allotransplantation in mice under FK506 immunosuppression. *Muscle Nerve* **17**: 1407–1415.
8. Skuk, D, Roy, B, Goulet, M, Chapdelaine, P, Bouchard, JP, Roy, R *et al.* (2004). Dystrophin expression in myofibers of Duchenne muscular dystrophy patients following intramuscular injections of normal myogenic cells. *Mol Ther* **9**: 475–482.
9. Gussoni, E, Pavlath, GK, Lanctot, AM, Sharma, KR, Miller, RG, Steinman, L *et al.* (1992). Normal dystrophin transcripts detected in Duchenne muscular dystrophy patients after myoblast transplantation. *Nature* **356**: 435–438.
10. Mendell, JR, Kissel, JT, Amato, AA, King, W, Signore, L, Prior, TW *et al.* (1995). Myoblast transfer in the treatment of Duchenne's muscular dystrophy. *N Engl J Med* **333**: 832–838.
11. Gussoni, E, Blau, HM and Kunkel, LM (1997). The fate of individual myoblasts after transplantation into muscles of DMD patients. *Nat Med* **3**: 970–977.
12. Beauchamp, JR, Morgan, JE, Pagel, CN and Partridge, TA (1999). Dynamics of myoblast transplantation reveal a discrete minority of precursors with stem cell-like properties as the myogenic source. *J Cell Biol* **144**: 1113–1122.
13. Hodgetts, SI, Beilharz, MW, Scalzo, AA and Grounds, MD (2000). Why do cultured transplanted myoblasts die *in vivo*? DNA quantification shows enhanced survival of donor male myoblasts in host mice depleted of CD4+ and CD8+ cells or Nk1.1+ cells. *Cell Transplant* **9**: 489–502.
14. Skuk, D, Caron, NJ, Goulet, M, Roy, B and Tremblay, JP (2003). Resetting the problem of cell death following muscle-derived cell transplantation: detection, dynamics and mechanisms. *J Neuropathol Exp Neurol* **62**: 951–967.
15. Skuk, D, Goulet, M, Roy, B and Tremblay, JP (2002). Efficacy of myoblast transplantation in nonhuman primates following simple intramuscular cell injections: toward defining strategies applicable to humans. *Exp Neurol* **175**: 112–126.
16. Skuk, D, Goulet, M, Roy, B, Chapdelaine, P, Bouchard, JP, Roy, R *et al.* (2006). Dystrophin expression in muscles of duchenne muscular dystrophy patients after high-density injections of normal myogenic cells. *J Neuropathol Exp Neurol* **65**: 371–386.
17. Skuk, D, Goulet, M, Roy, B, Piette, V, Cote, CH, Chapdelaine, P *et al.* (2007). First test of a "high-density injection" protocol for myogenic cell transplantation throughout large volumes of muscles in a Duchenne muscular dystrophy patient: eighteen months follow-up. *Neuromuscul Disord* **17**: 38–46.
18. Morgan, JE, Pagel, CN, Sherratt, T and Partridge, TA (1993). Long-term persistence and migration of myogenic cells injected into pre-irradiated muscles of mdx mice. *J Neurol Sci* **115**: 191–200.
19. Morgan, JE, Fletcher, RM and Partridge, TA (1996). Yields of muscle from myogenic cells implanted into young and old mdx hosts. *Muscle Nerve* **19**: 132–139.
20. Mueller, GM, O'Day, T, Watchko, JF and Ontell, M (2002). Effect of injecting primary myoblasts versus putative muscle-derived stem cells on mass and force generation in mdx mice. *Hum Gene Ther* **13**: 1081–1090.
21. Praud, C, Montarras, D, Pinset, C and Sebille, A (2003). Dose effect relationship between the number of normal progenitor muscle cells grafted in mdx mouse skeletal striated muscle and the number of dystrophin-positive fibres. *Neurosci Lett* **352**: 70–72.
22. Qu-Petersen, Z, Deasy, B, Jankowski, R, Ikezawa, M, Cummins, J, Pruchnic, R *et al.* (2002). Identification of a novel population of muscle stem cells in mice: potential for muscle regeneration. *J Cell Biol* **157**: 851–864.
23. Montarras, D, Morgan, J, Collins, C, Relaix, F, Zaffran, S, Cumano, A *et al.* (2005). Direct isolation of satellite cells for skeletal muscle regeneration. *Science* **309**: 2064–2067.
24. Sakamoto, M, Yuasa, K, Yoshimura, M, Yokota, T, Ikemoto, T, Suzuki, M *et al.* (2002). Micro-dystrophin cDNA ameliorates dystrophic phenotypes when introduced into mdx mice as a transgene. *Biochem Biophys Res Commun* **293**: 1265–1272.
25. Yoshimura, M, Sakamoto, M, Ikemoto, M, Mochizuki, Y, Yuasa, K, Miyagoe-Suzuki, Y *et al.* (2004). AAV vector-mediated microdystrophin expression in a relatively

small percentage of mdx myofibers improved the mdx phenotype. *Mol Ther* **10**: 821–828.
26. Fabb, SA, Wells, DJ, Serpente, P and Dickson, G (2002). Adeno-associated virus vector gene transfer and sarcolemmal expression of a 144 kDa micro-dystrophin effectively restores the dystrophin-associated protein complex and inhibits myofibre degeneration in nude/mdx mice. *Hum Mol Genet* **11**: 733–741.
27. Harper, SQ, Hauser, MA, DelloRusso, C, Duan, D, Crawford, RW, Phelps, SF *et al.* (2002). Modular flexibility of dystrophin: implications for gene therapy of Duchenne muscular dystrophy. *Nat Med* **8**: 253–261.
28. Acsadi, G, Dickson, G, Love, DR, Jani, A, Walsh, FS, Gurusinghe, A *et al.* (1991). Human dystrophin expression in mdx mice after intramuscular injection of DNA constructs. *Nature* **352**: 815–818.
29. Quenneville, SP, Chapdelaine, P, Rousseau, J, Beaulieu, J, Caron, NJ, Skuk, D *et al.* (2004). Nucleofection of muscle-derived stem cells and myoblasts with phiC31 integrase: stable expression of a full-length-dystrophin fusion gene by human myoblasts. *Mol Ther* **10**: 679–687.
30. Li, S, Kimura, E, Fall, BM, Reyes, M, Angello, JC, Welikson, R *et al.* (2005). Stable transduction of myogenic cells with lentiviral vectors expressing a minidystrophin. *Gene Ther* **12**: 1099–1108.
31. Quenneville, SP, Chapdelaine, P, Skuk, D, Paradis, M, Goulet, M, Rousseau, J *et al.* (2007). Autologous transplantation of muscle precursor cells modified with a lentivirus for muscular dystrophy: human cells and primate models. *Mol Ther* **15**: 431–438.
32. Bachrach, E, Li, S, Perez, AL, Schienda, J, Liadaki, K, Volinski, J *et al.* (2004). Systemic delivery of human microdystrophin to regenerating mouse dystrophic muscle by muscle progenitor cells. *Proc Natl Acad Sci USA* **101**: 3581–3586.
33. Sampaolesi, M, Torrente, Y, Innocenzi, A, Tonlorenzi, R, D'Antona, G, Pellegrino, MA *et al.* (2003). Cell therapy of alpha-sarcoglycan null dystrophic mice through intra-arterial delivery of mesoangioblasts. *Science* **301**: 487–492.
34. Sampaolesi, M, Blot, S, D'Antona, G, Granger, N, Tonlorenzi, R, Innocenzi, A *et al.* (2006). Mesoangioblast stem cells ameliorate muscle function in dystrophic dogs. *Nature* **444**: 574–579.
35. Fukada, S, Higuchi, S, Segawa, M, Koda, K, Yamamoto, Y, Tsujikawa, K *et al.* (2004). Purification and cell-surface marker characterization of quiescent satellite cells from murine skeletal muscle by a novel monoclonal antibody. *Exp Cell Res* **296**: 245–255.
36. Zammit, PS, Golding, JP, Nagata, Y, Hudon, V, Partridge, TA and Beauchamp, JR (2004). Muscle satellite cells adopt divergent fates: a mechanism for self-renewal? *J Cell Biol* **166**: 347–357.
37. Yablonka-Reuveni, Z and Rivera, AJ (1994). Temporal expression of regulatory and structural muscle proteins during myogenesis of satellite cells on isolated adult rat fibers. *Dev Biol* **164**: 588–603.
38. Cornelison, DD and Wold, BJ (1997). Single-cell analysis of regulatory gene expression in quiescent and activated mouse skeletal muscle satellite cells. *Dev Biol* **191**: 270–283.
39. Rando, TA and Blau, HM (1994). Primary mouse myoblast purification, characterization, and transplantation for cell-mediated gene therapy. *J Cell Biol* **125**: 1275–1287.
40. Burns, JC, Friedmann, T, Driever, W, Burrascano, M and Yee, JK (1993). Vesicular stomatitis virus G glycoprotein pseudotyped retroviral vectors: concentration to very high titer and efficient gene transfer into mammalian and nonmammalian cells. *Proc Natl Acad Sci USA* **90**: 8033–8037.
41. Nagai, T, Ibata, K, Park, ES, Kubota, M, Mikoshiba, K and Miyawaki, A (2002). A variant of yellow fluorescent protein with fast and efficient maturation for cell-biological applications. *Nat Biotechnol* **20**: 87–90.
42. Smythe, GM, Hodgetts, SI and Grounds, MD (2001). Problems and solutions in myoblast transfer therapy. *J Cell Mol Med* **5**: 33–47.
43. Hashimoto, N, Murase, T, Kondo, S, Okuda, A and Inagawa-Ogashiwa, M (2004). Muscle reconstitution by muscle satellite cell descendants with stem cell-like properties. *Development* **131**: 5481–5490.
44. Kobinger, GP, Louboutin, JP, Barton, ER, Sweeney, HL and Wilson, JM (2003). Correction of the dystrophic phenotype by *in vivo* targeting of muscle progenitor cells. *Hum Gene Ther* **14**: 1441–1449.
45. Mouly, V, Aamiri, A, Perie, S, Mamchaoui, K, Barani, A, Bigot, A *et al.* (2005). Myoblast transfer therapy: is there any light at the end of the tunnel? *Acta Myol* **24**: 128–133.
46. Kameya, S, Miyagoe, Y, Nonaka, I, Ikemoto, T, Endo, M, Hanaoka, K *et al.* (1999). Alpha1-syntrophin gene disruption results in the absence of neuronal-type nitric-oxide synthase at the sarcolemma but does not induce muscle degeneration. *J Biol Chem* **274**: 2193–2200.
47. Miyoshi, H, Blomer, U, Takahashi, M, Gage, FH and Verma, IM (1998). Development of a self-inactivating lentivirus vector. *J Virol* **72**: 8150–8157.
48. Naldini, L, Blomer, U, Gallay, P, Ory, D, Mulligan, R, Gage, FH *et al.* (1996). *In vivo* gene delivery and stable transduction of nondividing cells by a lentiviral vector. *Science* **272**: 263–267.
49. Dull, T, Zufferey, R, Kelly, M, Mandel, RJ, Nguyen, M, Trono, D *et al.* (1998). A third-generation lentivirus vector with a conditional packaging system. *J Virol* **72**: 8463–8471.

Research Signpost
37/661 (2), Fort P.O., Trivandrum-695 023, Kerala, India

Recent Advances of Skeletal Muscle Differentiation, 2008: ISBN: 978-81-308-0232-9
Editors: Kunihiro Tsuchida and Shin'ichi Takeda

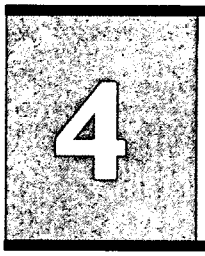

Side population (SP) cells and skeletal muscle differentiation

Yuko Miyagoe-Suzuki[1], Akiyoshi Uezumi[2] and Shin'ichi Takeda[1]
[1]Department of Molecular Therapy, National Institute of Neuroscience
National Center of Neurology and Psychiatry, 4-1-1 Ogawa-higashi, Kodaira
Tokyo 187-8502, Japan; [2]Institute for Comprehensive Medical Science
Division for Therapies Against Intractable Diseases, Fujita Health University
Toyoake, Aichi 470-1192, Japan

Abstract

Side population (SP) cells are isolated from various tissues by their ability to efficiently exclude the vital DNA dye Hoechst 33342. The clearance of the dye from the cells is thought to be mediated by ABC transporters. Bone marrow SP cells are rich in hematopoietic stem cells and have been demonstrated to participate in muscle fiber repair. Similarly, SP cells from skeletal muscle were shown to reconstitute the bone marrow of lethally irradiated mice and, at the same time, participate in muscle fiber regeneration.

Correspondence/Reprint request: Dr. Shin'ichi Takeda, Department of Molecular Therapy, National Institute of Neuroscience, National Center of Neurology and Psychiatry, 4-1-1 Ogawa-higashi, Kodaira, Tokyo 187-8502 Japan. E-mail: takeda@ncnp.go.jp

Several reports, however, suggest that muscle-derived SP cells are heterogeneous in origin, gene expression, and function. To further elucidate their functions and relationships with the other myogenic cells identified to date and their potential as a tool for cell-based therapy of muscular dystrophies, it might be necessary to refine the protocol for SP cell preparation and combine Hoechst staining with identification of several molecular markers.

Introduction

Duchenne muscular dystrophy (DMD) is a progressive, ultimately lethal X-linked muscle disorder, caused by mutations of the DMD gene [1], which encodes a large cytoskeletal protein, named dystrophin. Dystrophin forms the large dystrophin/dystrophin-associated protein complex at the sarcolemma of myofibers, linking the basal lamina and cytoskeleton. Dystrophin deficiency causes structural weakness of the sarcolemma. The defective sarcolemma easily ruptures under mechanical stress, leading to muscle fiber necrosis, and finally results in loss of myofibers and reduced contractile power.

Skeletal muscle regenerates when injured. Muscle satellite cells, which are muscle progenitor cells located between the muscle basal lamina and myofibers, are largely responsible for this activity [2], and were expected to be a cell source for cell-based therapy of DMD. However, transplantation of satellite cells or their progeny (myoblasts) into skeletal muscle showed insufficient regenerative efficiency, and failed to ameliorate the dystrophic phenotypes of animal models and DMD patients (reviewed in [3, 4]).

On the other hand, several reports have suggested that stem cell-like activities are found in non-satellite cell fractions derived from adult skeletal muscle or in non-muscle tissues and participate in muscle fiber regeneration [5-8]. Therefore, stem cells other than satellite cells could be an alternative cell source for cell-based therapy of muscle diseases such as DMD.

Among the myogenic stem cells reported to date are side population (SP) cells. Originally, SP cells were isolated from bone marrow as highly purified hematopoietic stem cells on the basis of their ability to efflux Hoechst 33342 dye [9]. Since then, cells with the SP phenotype have been found in a wide variety of mammalian tissues, cell lines, and tumor cells, some of which have shown to possess stem cell-like properties (reviewed in [10, 11]).

In this chapter, we review papers characterizing the properties of bone marrow SP cells and muscle SP cells. Importantly, many reports show that SP cells are highly heterogeneous. To correctly understand the therapeutic potential of SP cells, it might be necessary to combine Hoechst staining with identification of several cell surface markers and perform functional analysis using a limited number of SP cells.

I. Bone marrow side population cells

1. Discovery of SP cells as hematopoietic stem cells

Side population (SP) cells were discovered as highly purified hematopoietic stem cells [9]. While using Hoechst 33342 vital dye staining to study the cell cycle of bone marrow (BM) cells, Goodell et al. found that simultaneously displaying Hoechst fluorescence at two emission wavelengths (red 675 nm and blue 450 nm) localizes a distinct, small, non-stained cell population (0.1% of the total BM cells) that expresses markers of multipotent hematopoietic stem cells (HSC) (Sca1+lin$^{neg/low}$). *In vivo* competitive repopulation experiments revealed that HSC activities were enriched at least 1,000-fold in the SP fraction. The majority of BM-SP cells were not cycling: only 1-3 % of bone marrow SP cells were in S-G_2M stages of the cell cycle, whereas 20 % of main population (MP) cells were [9]. Because the SP fraction disappears when staining is performed in the presence of verapamil, Goodell et al. speculated that the exclusion of Hoechst 33342 by SP cells is an active process involving multidrug resistance protein (mdr) or mdr-like transporters [9]. Later, Zhou et al. demonstrated that breast cancer resistance protein (BCRP), also known ABCG2, is the molecular determinant of the SP phenotype [12, 13]. Interestingly, more detailed fractionation studies indicated that the SP tail can be further divided into subregions according to their dye efflux abilities, and that the tip of the SP cells (which have the highest Hoechst efflux activity) shows higher progenitor activity than the distal portion [14-16].

Although BM-SP cells are widely accepted as highly enriched hematopoietic stem cells, it seems that not all SP cells possess HSC activities [14]. Further, a recent study showed that hematopoietic stem cells are present in both SP and non-SP fractions [17]. Therefore, the properties of BM-SP and HSC cells are not completely identical.

2. Role of bone marrow SP cells in myogenesis

Ferrari et al. reported that BM-derived cells participated in repair of muscle fibers [8], suggesting that at least a fraction of myogenic precursor cells originate in the bone marrow, circulate throughout the body, and are mobilized to damaged muscle to regenerate muscle fibers. Later, Gussoni et al. injected BM-SP cells from wild-type male mice intravenously into lethally irradiated *mdx* female mice, and demonstrated that bone marrow SP cells contain both myogenic and hematopoietic precursors, i.e., they are multipotent stem cells with great plasticity [6]. These results gave us hope of recovering dystrophin expression in the whole musculature of patients with DMD by systemic delivery of BM-derived wild-type stem cells. Stimulated by these reports, researchers intensively investigated the properties of side population cells in bone marrow, especially the contribution of BM cells [18, 19] or BM-

SP cells [20] to muscle regeneration. BM cells and BM-SP cells prepared from GFP-transgenic or LacZ-expressing mice were indeed found to differentiate into muscle fibers *in vivo* after transplantation. Disappointingly, however, the percentage of myofibers formed by donor-derived cells delivered via the circulation was very low (1-2 %) and therapeutically not significant in most skeletal muscles.

Fusion or stepwise myogenic differentiation?

LaBarge and Blau reported that BM cells differentiate stepwise into myogenic precursor cells (e.g. satellite cells) and then, response to muscle injury, proliferate, fuse, and finally develop into mature myofibers [18]. Similarly, several reports suggested that BM-derived cells can differentiate into satellite cells [6, 19]. On the other hand, Sherwood et al. demonstrated that cells of bone marrow or hematopoietic origin did not give rise to functional adult myogenic progenitors [21]. Several reports provided evidence that the plasticity of hematopoietic stem cells shown in BM transplantation experiments can be explained simply as fusion events [22, 23]. Further, additional concerns have arisen from studies demonstrating that while BM cells or BM-SP cells are able to fuse with myofibers, a large proportion of incorporated cells do not actually enter the myogenic program [24, 25].

II. Muscle SP cells

1. Protocol for isolation of muscle SP cells

Although SP-like cells are found in mononuclear cells prepared from skeletal muscle (Figures 1 and 2), there are often discrepancies among reports in abundance, cell surface markers, and differential potentials of muscle SP cells (Table 1). This may be due to the many variables involved in the preparation and staining for isolation of SP cells by FACS. Montanaro et al. investigated the effects of isolation parameters on viability, yield, and phenotype of SP cells [26], and found that 1) the enzymatic dissociation procedure, 2) cell-counting method 3) Hoechst concentration, and 4) SP gating are important parameters to minimize the heterogeneity of SP cells prepared from bone marrow, skeletal muscle, or skin. They showed that when isolated using stringent criteria, muscle SP cells are CD45-negative and Sca1-positive, and show very low Hoechst uptake. The Hoechst concentration seems to be the most critical. For example, Hoechst 33342 staining at a concentration of 5 μg/ml allows contamination by CD45-positive and Sca-1-negative cells. In contrast, 12.5 μg/ml Hoechst reduces the yield of SP cells and increases the percentage of CD45-negative Sca-1-positive cells. Because the percentage of CD45-positive SP cells tends to decrease at higher concentrations of Hoechst 33342 in both BM and non-hematopoietic tissues, muscle- SP cells seem to